


Research Article

Climate variability in the northern Levant from the highly resolved Qadisha record (Lebanon) during the Holocene optimum

Carole Nehme^{a*} , Sophie Verheyden^b, Tobias Kluge^c, Fadi H. Nader^d, R. Lawrence Edwards^e, Hai Cheng^f, Elisabeth Eiche^c and Philippe Claeys^g

^aUMR IDEES 6266 CNRS, Université de Rouen-Normandie, Mont-Saint-Aignan, 76130 France; ^bDepartment of Earth History of Life, Royal Institute of Natural Sciences (RBINS), Brussels, Belgium; ^cInstitute of Applied Geosciences, Karlsruhe Institute of Technology, Karlsruhe, Germany; ^dIFP Énergies nouvelles, Direction des Sciences de la Terre et Technologies de l'Environnement, Rueil-Malmaison, 92500, France; ^eDepartment of Earth and Environmental Sciences, University of Minnesota, Minneapolis, Minnesota 55455, USA; ^fInstitute of Global Environmental Change, Xi'an Jiaotong University, Xi'an 710049, China and ^gAnalytical Environmental & Geo-Chemistry, Faculty of Science, Vrije Universiteit Brussel, Brussels, 1050, Belgium

Abstract

New stalagmites from Qadisha Cave (Lebanon) located at 1720 m above sea level provide a high-resolution and well-dated record for northern Mount Lebanon. The stalagmites grew discontinuously from 9.2 to 5.7 and at 3.5 ka, and they show a tendency to move from a more negative oxygen isotope signal at ~9.1 ka to a more positive signal at ~5.8 ka. Such a trend reflects a change from a wetter to a drier climate at high altitudes. The $\delta^{13}\text{C}$ signal shows rapid shifts throughout the record and a decreasing trend toward more negative values in the mid-Holocene, suggesting enhanced soil activity. In the short-term trend, Qadisha stalagmites record rapid dry/wet changes on centennial scales, with a tendency to more rapid dry events toward the mid-Holocene. Such changes are characterized by overall good agreement between both geochemical proxies and stalagmite growth and might be affected by the seasonal variations in snow cover. The Qadisha record is in good agreement with other Levantine records, showing more humid conditions from 9 to 7 ka. After 7 ka, a drier climate seems to affect sites at both low- and high-altitude areas. The Qadisha record reflects uniquely mountainous climate characteristics compared with other records, specifically the effect of snow cover and its duration regulating the effective infiltration.

Keywords: Qadisha, Holocene, Speleothems, Geochemistry, Snow cover

(Received 27 December 2022; accepted 8 May 2023)

INTRODUCTION

The impact of future climatic change in the eastern Mediterranean (EM), a region already exposed to severe agricultural and environmental water stress, must be better constrained and may be assessed by investigating past climatic variability (Masson-Delmotte et al., 2013). The climate of the EM is influenced by weather systems originating from the North Atlantic Ocean, passing from Europe to the Mediterranean Sea. In the EM region, many records from lake and marine cores (Rohling et al., 2002; Emeis et al., 2003; Jones and Roberts, 2008; Almogi-Labin et al., 2009; Develle et al., 2010) and speleothems (Bar-Matthews et al., 2003; Verheyden et al., 2008; Cheng et al., 2015) have been used to define past climate conditions. Regional paleoclimate records suggest that the region is sensitive to large-amplitude glacial–interglacial changes and climatic fluctuations on millennial to decadal timescales (Bar-Matthews et al., 2003; Almogi-Labin et al., 2009; Bar-Matthews and Ayalon, 2011). However, this sensitivity is unequal among regions because of the

heterogeneity of the EM climate (Fig. 1) over short distances (Ulbrich et al., 2012). The precipitation distribution shows high spatiotemporal variability, with most of the effective moisture occurring during winter–spring seasons and being concentrated in mountainous regions. Confidently reconstructing this variability requires a dense network of precisely dated and highly resolved paleoclimate records. Past spatiotemporal climate variability in the EM is still poorly documented due to unevenly distributed records (Burstyn et al., 2019).

In the Levantine region stretching from southern Taurus mountains to southern Negev desert and the island of Cyprus, many studies cover the Holocene period, but few are well dated (Bar-Matthews et al., 2003; Cheng et al., 2015) or record rapid climate changes (RCC). Some are located along the coast at low altitudes like Jeita Cave or Zalmon Cave, other records such as Soreq and West Jerusalem Caves are located at mid-altitudes (western flanks of the Judean plateaus). Some lake or marsh records are located in the rain shadow of the Levantine mountains (e.g., the Dead Sea, the Ammiq marsh in the Beqaa inner plain, the Ghab depression). Among the records covering the Holocene, a few are located in high mountainous areas, such as Mizpe Shelagim Cave in Mount Hermon and Incesu Cave in the Taurus Mountains (Turkey). In the central Levant, Mt. Lebanon (3088 m) is an imposing range facing the moisture coming

*Corresponding author: Carole Nehme; Email: carole.nehme@univ-rouen.fr

Cite this article: Nehme C, Verheyden S, Kluge T, Nader FH, Edwards RL, Cheng H, Eiche E, Claeys P (2024). Climate variability in the northern Levant from the highly resolved Qadisha record (Lebanon) during the Holocene optimum. *Quaternary Research* 118, 180–194. <https://doi.org/10.1017/qua.2023.24>



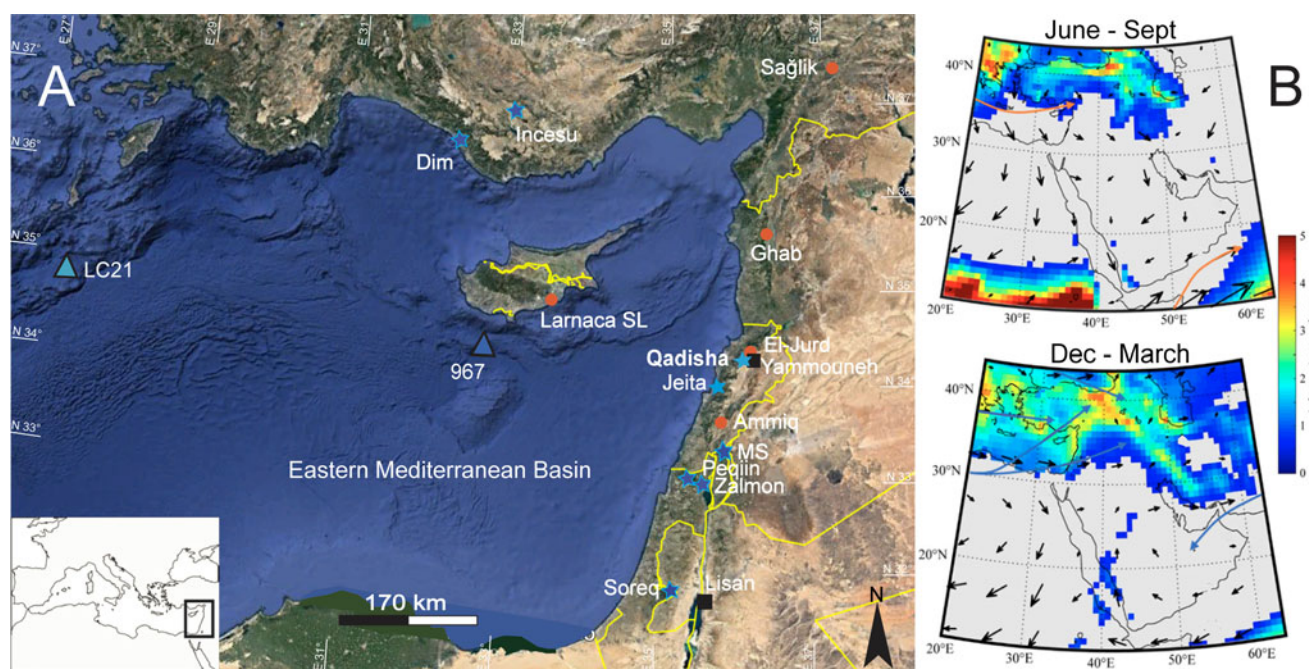


Figure 1. (A) Location of Qadisha Cave (this study) and other paleoclimatic records spanning the Holocene: Lisan lake (Torfstein et al., 2013a, 2013b), Soreq Cave (Bar-Matthews et al., 2003; Burstyn et al., 2022), Zalmou Cave (Keinan et al., 2019), Peqiin Cave (Bar-Matthews et al., 2003), Mizpe Shelagim (MS) Cave (Ayalon et al., 2013), Ammiq peat record (Hajjar et al., 2010), Jeita Cave (Verheyden et al., 2008; Cheng et al., 2015), Yammouneh basin (Develle et al., 2010), El-Jurd peat record (Cheddadi and Khater, 2016), Ghab core (Van Zeist and Woldring, 1980; Yasuda et al., 2000), Sağlik peat (Sekeryapan et al., 2020), Incesu Cave (Erkan et al., 2022), Dim Cave (Ünal-Imer et al., 2015), LC21 (Grant et al., 2012), and ODP 967 (Emeis et al., 2003; Scrivner et al., 2004). (B) Maps showing seasonal precipitation amounts in the wider eastern Mediterranean region. Panels at the right illustrate seasonal precipitation amounts from June to September and from December to March, respectively. Gray areas indicate regions where the daily precipitation amount is below 0.5 mm. Data retrieved from the ERA-Interim reanalysis data set (1979 to 2015 CE) (Berrisford et al., 2011).

from the Mediterranean and creates therefore a peculiar local climate system in Lebanon. None of the records spanning the Holocene were retrieved in areas located at high altitude, except for the El-Jurd marsh (Cheddadi and Khater, 2016) and Yammouneh lake records, which both provide low-resolution (millennial-scale) data. To analyze the effect of the mountainous climate and its variability during the Holocene, a reconstruction of past climate variations from highly resolved archives such as speleothems is needed. These secondary cave deposits (e.g., stalagmites) are currently considered to be the most suitable terrestrial archives for establishing high-resolution proxy time series in paleoclimate research (Genty et al., 2003; Cheng et al., 2012; Fairchild and Baker, 2012).

We report new stalagmite stable isotope data ($\delta^{13}\text{C}$, $\delta^{18}\text{O}$) from Qadisha Cave (Lebanon) located at 1720 m above sea level (m asl), which provides a high-resolution and well-dated record for northern Mt. Lebanon covering the time period from 9 to 5 ka. The combined measurements of calcite $\delta^{13}\text{C}$ and $\delta^{18}\text{O}$ and trace elements enable us to characterize the regional climate trend versus the local mountainous effect on high-altitude records. Isotope measurements of fluid inclusion water (δD , $\delta^{18}\text{O}_w$) provide insights into the hydrologic cycle and allow an estimation of mineral formation temperatures for the Holocene optimum at the high-altitude Qadisha Cave.

STATE OF THE ART

During the past decades, several synthesis reports were prepared on paleoclimate studies in the EM (Robinson et al., 2006; Finné et al., 2011; Burstyn et al., 2019), compiling many marine

(Rossignol-Strick and Paterne, 1999; Kallel et al. 2000; Emeis et al. 2003; Almogi-Labin et al., 2009) and terrestrial records spanning the Holocene (Frumkin et al. 2000; Bar-Matthews et al. 2003; Verheyden et al., 2008; Develle et al. 2010; Rowe et al., 2012; Ayalon et al., 2013; Cheng et al., 2015; Gasse et al., 2015; Ünal-Imer et al., 2015; Cheddadi and Khater, 2016; Flohr et al., 2017; Carolin et al., 2019; Sinha et al., 2019; Jacobson et al., 2021; Burstyn et al., 2022; Erkan et al., 2022). Focusing more on the Levantine coast, from the Sinai and Negev Deserts to the southern flanks of the Taurus Mountains in Turkey, and including Cyprus, studies have revealed a general climatic state of a wet and warm Early Holocene from ~ 10 to ~ 6 ka during maximum summer insolation, coeval with the deposition of Sapropel S1. Sapropels are organic-rich layers deposited during periods of increased discharge of the river Nile (Rossignol-Strick and Paterne, 1999; Kallel et al. 2000). This processional timescale effect results in isotopically lighter sea-surface water due to the contribution of the $\delta^{18}\text{O}$ -depleted Nile influx into the EM sea basin. This isotopic source effect is expressed in the Soreq, Peqiin (Bar-Matthews et al., 2003; Bar-Matthews and Ayalon, 2011; Burstyn et al., 2022), and Jeita Cave records (Verheyden et al., 2008; Cheng et al., 2015), with more negative oxygen isotope values following the depletion of sea-surface $\delta^{18}\text{O}$ as resolved from planktonic foraminifera (Grant et al., 2016). In the southern Taurus Mountains, both Dim (Unal-Imer et al., 2015) and Incesu Cave records (Erkan et al., 2022) show a trend toward more depleted $\delta^{18}\text{O}$ from ~ 10 to ~ 8 ka. Although the isotopic composition of the EM source is considered to have a primary effect on the $\delta^{18}\text{O}$ signal of the terrestrial records, the isotopic $\delta^{18}\text{O}$ depletion is amplified by

increased rainfall (Emeis et al., 2003; Almogi-Labin et al., 2009), also leading to more negative $\delta^{18}\text{O}$ values. This effect has been invoked for the Early Holocene in some speleothem records (Burstyn et al., 2019) and the Yammouneh polje record (Develle et al., 2010).

The distribution of rainfall and how it changed during the Holocene were not coeval along the Levantine coast. Regional variations in the rainfall amount cause isotopic variations, as attested by cave climate monitoring studies (Bar-Matthews et al., 1996; Ayalon et al., 1998, 2004; Nehme et al., 2019). Cave water isotopic values are biased toward the main infiltration period, which is the winter–spring season (Nehme et al., 2019, 2020). The isotopic signal of the infiltration water is transferred into the cave calcite. Rapid seasonal, decadal, or centennial isotopic variations in speleothems are therefore more likely related to rainfall amount changes (Bar-Matthews et al., 1996; Orland et al., 2014; Nehme et al., 2019), as cave temperature would not vary strongly on seasonal, annual, or, in deep, less-ventilated caves, decadal scales. The impact of temperature on the calcite $\delta^{18}\text{O}$ values is about 0.2‰ per 1°C change (Demeny et al., 2010; Tremaine et al., 2011; Daëron et al., 2019), whereas a 200 mm change in the annual rainfall amount could cause a change in the $\delta^{18}\text{O}$ of rainfall, and therefore of the infiltrating water by 1‰, as measured at the Soreq Cave site by Bar Matthews et al. (2003).

Develle et al. (2010) and Cheng et al. (2015) found contrasting patterns of climatic variability between records from the northern and southern Levant. Cheng et al. (2015) emphasize an out-of-phase pattern between records from the northern Levant relative to the Dead Sea Basin (DSB). The contrasting pattern of precipitation is likely due to enhanced warm southerly–southwesterly flow, which intensifies winter–spring precipitation over the northern Levant (Brayshaw et al., 2011). Furthermore, the contrasting north–south precipitation pattern persists on millennial to centennial timescales, linked potentially to an enhanced (weakened) meridional circulation, which results in a wet (dry) northern (southern) Levant (Xoplaki et al., 2004), expressed by a contrasting RCC between Jeita isotopic variations and DSB levels (Cheng et al., 2015).

Cheng et al. (2015) emphasized the relevance of distinct effective infiltration (precipitation–evaporation [P-E]) effects, enhanced by local factors (topography, vegetation) between the northern and southern Levant, in parallel with changes in meridional circulation patterns. This interpretation, previously proposed by Develle et al. (2010), focuses on effective rainfall, related to P-E in both soil and epikarst that affects water supply to caves (infiltration) and lakes (drainage) and thus explains differences in water balances between sites. Indeed, Develle et al. (2010) stressed the different timing of RCC in the northern and southern Levant.

According to the Jeita Cave and Aammq marsh records (Hajjar et al., 2010), the major shift from humid to general dry conditions occurred around 6 ka, which is different than in the Dead Sea, the level of which was extremely low during the entire Holocene compared with the last glacial maximum (LGM). Migowski et al. (2006) do not exclude the possibility that those humid conditions relative to modern times prevailed in the DSB during the Early Holocene, but the water balance contrast between the Yammouneh and DSB records relies on different P-E conditions in both regions. For example, the Yammouneh record (Develle et al., 2010) does not reveal proxy evidence for a drought around 8 ka as observed in the Jeita record (Cheng et al., 2015) at lower altitude. More to the south, the 8.2 ka

event was identified in the Soreq record (Bar-Matthews et al., 2003), but was not interpreted as a drought.

Effective infiltration (P-E) also influences proxies related to local soil and epikarst conditions, such as $\delta^{13}\text{C}$ in carbonates. Such proxies, conditioned by vegetation cover and soil microbial productivity, are additionally influenced by CO_2 degassing and prior calcite precipitation (PCP) related to changing cave drip rates (Fohlmeister et al., 2020). In the EM region, a contrasting pattern of hydroclimate variability between the northern and southern Levant is exemplified by comparison of the $\delta^{13}\text{C}$ profile of Jeita with Peqiin and Soreq records. Although the Jeita and Peqiin records show similar $\delta^{13}\text{C}$ and $\delta^{18}\text{O}$ isotopic trends, a notable heavy excursion in the Soreq $\delta^{13}\text{C}$ record from ~10 to ~7 ka presents an opposite trend relative to the Jeita $\delta^{13}\text{C}$ curve. This positive Soreq $\delta^{13}\text{C}$ event is interpreted to reflect an extremely wet period in the southern Levant, partially because of its association with lighter $\delta^{18}\text{O}$ values (Bar-Matthews and Ayalon, 2011). Cheng et al. (2015) challenge this interpretation and suggest that the Soreq record could reflect drier conditions during the Early Holocene, consistent with low Dead Sea levels. The recent publication of Burstyn et al. (2022) follows the interpretation of Bar-Matthews and Ayalon (2011) and involves a complex opposite response system of magnetic particle influx to rainfall to demonstrate the coupling between the inflow of magnetic particles (IRM_{flux}) and $\delta^{13}\text{C}$ in Soreq speleothems. The contrasting climates between the northern and southern Levant are therefore still under debate, and factors in the local P-E response to the synoptic climate systems (e.g., topography) are still not well constrained, mainly due to different interpretations of the $\delta^{13}\text{C}$ response to water availability.

CURRENT CLIMATIC SETTINGS OF THE LEVANT

Today, the Levant region is mainly influenced by the midlatitude westerlies, which originate from the Atlantic Ocean, forming a series of subsynoptic low-pressure systems across the Mediterranean Sea (Gat et al., 2003; Ziv et al., 2010). In winter, cold air plunging south over the relatively warm Mediterranean enhances cyclogenesis, creating the Cyprus Low (Alpert et al., 2005). Moist air is then driven onshore, generating intense orographic rainfall across Mt. Lebanon, Mt. Hermon, and the Syrian mountains in the northern Levant. In summer, the westerly belt is shifted to the north, following the northern shift of the North African subtropical high pressures, and the region experiences hot and dry conditions with more southerly winds. In Lebanon, the annual rainfall varies between 700 and 1000 mm along the coastline and more than 1400 mm in the mountains. Average snow coverage is 5 months from December to April (Shabaan and Houhou, 2015) in basins located at mid-altitudes (1200–2000 m) and up to 7 months from December to June (Fayad and Gascoin, 2020) in high-altitude basins (>2500 m). As a consequence of this circulation system, the climate is seasonal with wet winters (November to February) and dry, hot summers (May to October), with a significant influence of snow coverage (up to 75%) on the water supply budget in karst networks and springs at high altitudes (Koeninger et al., 2017).

A general west–east gradient in rainfall (amount, isotopic composition) from the Lebanese coastline to the inner Beqaa plain is evident in the published local meteoric water line (Aouad-Rizk et al., 2005) as a consequence of the altitudinal effects related to Rayleigh distillation processes (Dansgaard, 1964; Rozanski et al., 1993). This gradient is mirrored in the cave stream and drip-water

isotopic composition (Nehme et al., 2019), with a clear altitudinal gradient from the coastline to the highest Mt. Lebanon peaks. The north–south gradient at Mt. Lebanon and to the south is also expressed in the isotopic composition and amount of rainfall. The studies of Aouad-Rizk et al. (2005), Gat et al. (2003), and Saad et al. (2005) showed more positive isotopic rainfall values and a lower rainfall amount toward the south, impacting the water balance (P-E) and effective infiltration in karstic systems along the Levantine coast and mountain chains.

CAVE SITE AND SAMPLE DESCRIPTION

Qadisha Cave (34°14'38"N, 36°02'11"E) is located 1720 m asl in the northern part of Mt. Lebanon (Fig. 1), in the vicinity of the highest peak of the mountain chain (Mt. Makmel), which reaches 3088 m asl. The latter, with its northeast–southwest direction, faces the EM Basin. The cave develops in Quaternary deposits derived from dolomitized Cretaceous limestone, located in the vicinity of the Qadisha catchment basin (Dubertret, 1975; Nader et al., 2006). The basin is fed by ample snowmelt and has a mean elevation of 2244 m. The duration of snow cover is variable across years and reaches 6 to 7 months in the Qadisha water catchment basin (Telesca et al., 2014; Fayad and Gascoïn, 2020). The cave is horizontal, with more than 1076 m of explored galleries, comprising an upper relict part and lower active part with a permanent spring (discharge rate up to 1 m³/s) (Edgell, 1997). Qadisha Cave was partially transformed into a tourist cave in 1934 (first show cave in Lebanon). It is located near the cedar forest of Bsharreh, which is believed to have covered a wider area in the past. Today, the Quaternary deposits above the cave, consisting mainly of scree and cemented rock debris, are covered with shrub vegetation (Dubertret, 1975). A previous monitoring study in the cave (Nehme et al., 2019) showed a mean cave air temperature of 9.0 ± 0.5°C and a pCO₂ concentration of 600 ppmv. Water percolation through the cave persists generally throughout the year. Two speleothems, Qad-1 and Qad-2, were retrieved from the upper gallery of the cave, which hosts many active stalagmites.

METHODS

²³⁰Th dating

The chronologies of Qad-1 and Qad-2 were established using 10 and 9 ²³⁰Th dates, respectively (Table 1). Exploratory ²³⁰Th dating was performed first at Xi'an Jiaotong University (China) in 2011 and 2014, and the rest was completed at the University of Minnesota (USA) in 2018, by using Thermo-Finnigan Neptune/Neptune Plus multi-collector inductively coupled plasma mass spectrometers. The methods in both laboratories were identical (Cheng et al., 2013). Standard chemistry procedures (Edwards et al., 1987) were used to separate uranium and thorium. A triple-spike (²²⁹Th-²³³U-²³⁶U) isotope dilution method was used to correct instrumental fractionation and to determine U/Th isotopic ratios and concentrations (Cheng et al., 2013). U and Th isotopes were measured on a MassCom multiplier behind the retarding potential quadrupole in the peak-jumping mode using standard procedures (Cheng et al., 2013). Uncertainties in U/Th isotopic measurements were calculated offline at 2σ, including corrections for blanks, multiplier dark noise, abundance sensitivity, and contents of the same nuclides in spike solution. Corrected ²³⁰Th ages assume an initial ²³⁰Th/²³²Th atomic ratio

of 4.4 ± 2.2 × 10⁻⁶, the values for a material at secular equilibrium with a bulk earth ²³²Th/²³⁸U value of 3.8 (Cheng et al., 2013).

Calcite and water stable isotopes measurements

Samples for stable isotopic analyses were taken along the growth axes of Qad-1 and Qad-2 stalagmites (Fig. 2) for δ¹³C and δ¹⁸O measurements. Overall, 230 samples were measured in both stalagmites. Samples were drilled along the stalagmite growth axis at 2.5 mm resolution using a Merchantek Micromill mounted on a Leica microscope, with a 0.3 mm resolution for specific parts. Between every sample, the drill bit and sampling surface were cleaned with compressed air. The samples were analyzed using a Nu Carb carbonate device coupled to a Nu Perspective mass spectrometer (MS) at Vrije Universiteit Brussel (Belgium). Parts of the samples were measured at the Laboratory for Environmental and Raw Material Analysis at the Karlsruhe Institute of Technology (Germany), using a Thermo Gasbench II connected to a DELTA V IRMS in continuous-flow mode. All δ¹⁸O and δ¹³C values are calibrated against Vienna Pee Dee Belemnite (VPDB) and are reported in per mil (‰). Analytical uncertainties were better than 0.1‰ (1σ) for oxygen and 0.05‰ (1σ) for carbon on both instruments. Percolation and stream waters as well as recent calcite samples underneath active drip water were collected previously from Qadisha Cave in 2011 and 2014 (Nehme et al., 2019).

Trace element data

Elemental abundances were determined by laser ablation-inductive coupling plasma-MS (LA-ICP-MS), at the Institute for Geosciences, Johannes Gutenberg University Mainz (Germany), using an ESI NWR193 ArF excimer LA system equipped with the TwoVol² ablation cell, operating at 193 nm wavelength, coupled to an Agilent 7500ce quadrupole ICP-MS. Ablation was performed in line scan mode and surfaces were pre-ablated before each line scan to prevent potential surface contamination. Line scans were performed at a scan speed of 10 μm/s, using a spot size of 110 μm and a laser repetition rate of 10 Hz. Laser energy on the samples was about 3 J/cm². Measured ion intensities were monitored in time-resolved mode, and background intensities were measured for 15 s. Synthetic glass NIST SRM 612 was used to calibrate element concentrations, with the preferred values given in the GeoReM database being applied (Jochum et al., 2005, 2012). Quality-control materials (QCMs) (USGS MACS-3 and USGS BCR-2G) were used to monitor the accuracy and precision of the LA-ICP-MS analysis and calibration strategy. Raw data were processed using TERMITE (Mischel et al., 2017), an R script for data reduction. The internal standard was ⁴³Ca, applied as an internal standard, at a Ca concentration of 390,000 μg/g. The values for trace element results are reported in the GeoReM database for the QCMs. Element concentrations determined for the QCMs had a precision of <0.02% (1σ).

Fluid inclusion stable isotope (H-O) analyses

Five calcite samples, from three levels in the Qad-2 stalagmite were measured using a custom-built extraction line connected to a Picarro L2130i analyzer using cavity ring down spectroscopy. This technique allows simultaneous measurement of hydrogen and oxygen isotopes for minute water amounts released from calcite. The extraction line follows the design of Affolter et al. (2014)

Table 1. ²³⁰Th dating results of stalagmites Qad-stm1 and Qad-stm2 (error is given as 2 SE).^a

| Sample no. | Depth mm | ²³⁸ U ppb | ²³² Th ppt | ²³⁰ Th / ²³² Th (atomic × 10 ⁻⁶) | δ ²³⁴ U ^b (measured) | ²³⁰ Th / ²³⁸ U (activity) | ²³⁰ Th Age (a) (uncorrected) | ²³⁰ Th Age (a) (corrected) ^c | δ ²³⁴ U _{Initial} ^{**} (corrected) | ²³⁰ Th age (yr CE) ^d (corrected) |
|--------------------------|-------------|-------------------------|--------------------------|---|---|--|--|---|--|---|
| Qad-stm1-0 | 2 | 435.0 ± 1.0 | 3591 ± 72 | 85 ± 2 | 353.7 ± 2.2 | 0.0426 ± 0.0002 | 3848 ± 19 | 3307 ± 127 | 357 ± 2 | 3247 ± 127 |
| Qad-stm1-8 | 7 | 606.5 ± 0.6 | 132 ± 3 | 5739 ± 140 | 442.4 ± 1.5 | 0.0756 ± 0.0003 | 5853 ± 28 | 5848 ± 28 | 450 ± 1 | 5780 ± 28 |
| Qad-stm1-7 | 26 | 575.7 ± 0.9 | 97 ± 3 | 7502 ± 240 | 444.3 ± 2.2 | 0.0764 ± 0.0004 | 5914 ± 30 | 5911 ± 30 | 452 ± 2 | 5843 ± 30 |
| Qad-stm1-6 | 46 | 615.3 ± 1.0 | 122 ± 3 | 6432 ± 183 | 450.6 ± 2.0 | 0.0774 ± 0.0004 | 5966 ± 29 | 5962 ± 29 | 458 ± 2 | 5894 ± 29 |
| Qad-stm1-5 | 65 | 665.4 ± 0.7 | 361 ± 8 | 2329 ± 50 | 445.7 ± 1.7 | 0.0767 ± 0.0003 | 5929 ± 24 | 5918 ± 25 | 453 ± 2 | 5850 ± 25 |
| Qad-stm1-4 | 77 | 535.7 ± 1.0 | 466 ± 10 | 1472 ± 31 | 437.3 ± 2.7 | 0.0777 ± 0.0004 | 6045 ± 33 | 6028 ± 35 | 445 ± 3 | 5960 ± 35 |
| Qad-stm1-3 | 96 | 572.6 ± 0.6 | 352 ± 7 | 2126 ± 46 | 432.1 ± 1.5 | 0.0792 ± 0.0003 | 6185 ± 28 | 6173 ± 29 | 440 ± 2 | 6105 ± 29 |
| Qad-stm1-2 | 101 | 546.2 ± 0.6 | 66 ± 2 | 11419 ± 389 | 441.9 ± 1.8 | 0.0840 ± 0.0003 | 6528 ± 25 | 6525 ± 25 | 450 ± 2 | 6457 ± 25 |
| Qad-stm1-1 | 115 | 643.7 ± 1.1 | 1156 ± 23 | 792 ± 16 | 433.5 ± 2.2 | 0.0863 ± 0.0003 | 6748 ± 28 | 6711 ± 38 | 442 ± 2 | 6643 ± 38 |
| Qad-stm1-00 ^e | 128 | 639.0 ± 2.0 | 978 ± 20 | 902 ± 18 | 428.1 ± 2.6 | 0.0838 ± 0.0003 | 6573 ± 24 | 6542 ± 32 | 436 ± 3 | 6482 ± 32 |
| Qad-Stm2-5 | 6 | 558.6 ± 1.5 | 194 ± 4 | 45 ± 3 | 303.3 ± 2.1 | 0.0009 ± 0.0001 | 79 ± 5 | 71 ± 7 | 303 ± 2 | 5 ± 7 |
| Qad-stm2-4 | 13 | 297.6 ± 0.3 | 193 ± 4 | 2309 ± 51 | 397.4 ± 1.7 | 0.0907 ± 0.0004 | 7294 ± 36 | 7281 ± 37 | 406 ± 2 | 7213 ± 37 |
| Qad-stm2-3 | 25 | 621.7 ± 0.6 | 316 ± 6 | 3161 ± 65 | 406.2 ± 1.4 | 0.0973 ± 0.0002 | 7794 ± 22 | 7783 ± 23 | 415 ± 1 | 7715 ± 23 |
| Quad 2-8.2 | 28.2 | 351.8 ± 0.3 | 255 ± 6 | 2284 ± 50 | 423.4 ± 1.6 | 0.1003 ± 0.0004 | 7937 ± 38 | 7922 ± 39 | 433 ± 2 | 7851 ± 39 |
| Qad-stm2-2 | 30 | 336.4 ± 0.5 | 87 ± 2 | 6980 ± 178 | 457.5 ± 2.1 | 0.1093 ± 0.0004 | 8466 ± 32 | 8461 ± 33 | 469 ± 2 | 8393 ± 33 |
| Qad stm2-8.6 | 36 | 367.1 ± 0.3 | 284 ± 6 | 2422 ± 52 | 483.2 ± 1.6 | 0.1138 ± 0.0004 | 8667 ± 35 | 8652 ± 36 | 495 ± 2 | 8581 ± 36 |
| Qad-stm2-8 | 49 | 499.2 ± 0.7 | 62 ± 2 | 15661 ± 580 | 481.2 ± 2.2 | 0.1186 ± 0.0004 | 9062 ± 35 | 9060 ± 35 | 494 ± 2 | 8992 ± 35 |
| Qad-stm2-7 | 67 | 582.4 ± 0.8 | 188 ± 4 | 6121 ± 144 | 484.8 ± 2.1 | 0.1200 ± 0.0004 | 9153 ± 34 | 9147 ± 34 | 497 ± 2 | 9079 ± 34 |
| Qad-stm2-6 | 80 | 566.7 ± 0.8 | 379 ± 8 | 2970 ± 63 | 489.1 ± 2.1 | 0.1206 ± 0.0004 | 9167 ± 34 | 9154 ± 35 | 502 ± 2 | 9086 ± 35 |
| Qad-Stm2-1 | 106 | 545.4 ± 0.9 | 207 ± 4 | 5220 ± 106 | 472.7 ± 1.4 | 0.1199 ± 0.0002 | 9218 ± 20 | 9211 ± 21 | 485 ± 1 | 9145 ± 21 |

^aU decay constants: $t^{238} = 1.55125 \times 10^{-10}$ (Jaffey et al., 1971) and $t^{234} = 2.82206 \times 10^{-6}$ (Cheng et al., 2013). Th decay constant: $t^{230} = 9.1705 \times 10^{-6}$ (Cheng et al., 2013).

^b $d^{234}U = ([^{234}U/^{238}U] \text{ activity} - 1) \times 1000$.

^c $d^{234}U$ initial was calculated based on ²³⁰Th age (T), i.e., $d^{234}U_{\text{initial}} = d^{234}U_{\text{measured}} \times e^{\lambda_{234} \times T}$.

^dCorrected ²³⁰Th ages assume the initial ²³⁰Th/²³²Th atomic ratio of $4.4 \pm 2.2 \times 10^{-6}$. Those are the values for a material at secular equilibrium, with the bulk earth ²³²Th/²³⁸U value of 3.8.

^eThe errors are arbitrarily assumed to be 50%. Ages are defined as the year before 1950 CE.

^fAge considered as outlier.

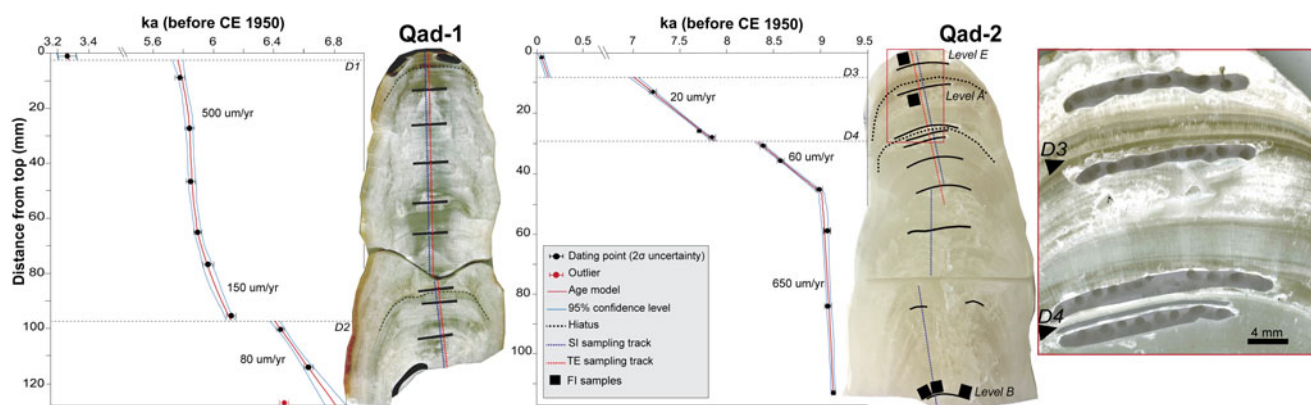


Figure 2. Age model of both Qadisha-1 (Qad-1) and Qadisha-2 (Qad-2) stalagmites using StalAge (Scholz and Hoffmann, 2011). Sampling track for stable isotopes, trace elements, and locations of fluid inclusions (squares) along the growth axis are shown on each stalagmite. Red rectangle in the upper part of the Qad-2 stalagmite shows a high-resolution image of discontinuities D3 and D4 along the growth axis. F1, fluid inclusions; SI, stable isotope; TE, trace elements.

and is described in detail in Weissbach et al. (2023). In brief, the calcite samples were hydraulically crushed, and the released fluid inclusion water instantly vaporized in the heated extraction system and transferred to the analyzer. Reference water injections with known $\delta^{18}\text{O}$ and δD values were used for calibration and quality control. Glass capillaries (microliter size) were used for high-precision water amount calibration and isotopic control. The precision of fluid inclusion water analyses is dependent on the released water amount and is 0.5‰ for $\delta^{18}\text{O}$ and 1.2‰ for $\delta^2\text{H}$, if fluid water amounts are $>0.2\ \mu\text{l}$, and reaches 0.1–0.3‰ for $\delta^{18}\text{O}$ and 0.2–0.7‰ for $\delta^2\text{H}$ for fluid water amounts $>1\ \mu\text{l}$ (Weissbach et al., 2023).

RESULTS

Petrography and chronology

Over most sections, both samples of 11 cm for Qad-1 and 13 cm for Qad-2 display a translucent to whitish calcite with a columnar fabric along their growth axis. Both stalagmites are highly laminated. With the aid of a camera mounted on a Leica Microscope, images of laminae were taken at several depths, and the thickness of each was measured. Layer thickness of laminae varied between 60 and 280 μm . The laminar growth is irregular and alternates between thin (60–70 μm) to thick laminae (200–280 μm).

A total of 19 U/Th ages were obtained from stalagmites Qad-1 and Qad-2 (Table 1). The age distribution based on the StalAge model (Scholz and Hoffmann, 2011) indicates that stalagmite Qad-1 grew from ca. 6.643 ± 0.038 to 3.247 ± 0.127 ka, including two discontinuities (Fig. 2). The first discontinuity, D1, ranges from 5.787 to 3.247 ka (extrapolated ages), and D2 covers a shorter period from 6.408 to 6.108 ka (extrapolated ages). Qad-2 grew from 9.145 ± 0.021 to 0.005 ± 0.007 ka, including two discontinuities: D3 (7.016 to 0.005 ka) and D4 (7.844 to 8.326 ka). The age model of Qad-1 was constructed with eight ages, with one other age (Qad-stm1-00) considered to be an outlier. The latter is sampled on the edge of the growth axis and is not in stratigraphic order with the other dating points. At the base of Qad-1, the growth rate is around 60 $\mu\text{m}/\text{yr}$, evolving to a higher rate around 150 $\mu\text{m}/\text{yr}$ and up to 500 $\mu\text{m}/\text{yr}$ in the upper part of the stalagmite. For the Qad-2 stalagmite, all the ages are in stratigraphic order and were used in the calculation

of the age model. The growth rate at the base of Qad-2 is very high, reaching 650 $\mu\text{m}/\text{yr}$ and is reduced to 60 and 20 $\mu\text{m}/\text{yr}$ in the middle and upper part of the stalagmite.

Stable isotopic composition of calcite, modern water, and fluid inclusions

Calcite $\delta^{18}\text{O}$ and $\delta^{13}\text{C}$ values were analyzed at a multi-annual to decadal resolution. The $\delta^{18}\text{O}$ values for the Qadisha record (Fig. 3) range from -5.7‰ to -7.5‰ , with a mean of -6.8‰ . The $\delta^{13}\text{C}$ values range from -6.2‰ to -8.6‰ , around a mean of -7.5‰ . Both $\delta^{18}\text{O}$ and $\delta^{13}\text{C}$ values generally covary during the entire period from ~ 9.1 to ~ 5.7 ka but are distinct in the medium- and long-term trends. For example, the $\delta^{18}\text{O}$ values show an overall trend toward more positive values from the Early to the Middle Holocene, unlike the $\delta^{13}\text{C}$ values, which show a trend toward more negative values when reaching the mid-Holocene. Significant variations are noticeable in the stable isotope curves, with clear $\delta^{18}\text{O}$ and $\delta^{13}\text{C}$ excursions around ~ 9.1 , ~ 8.9 , ~ 7.7 , ~ 7.4 – 7.2 , ~ 6.5 , and ~ 5.9 ka.

Stable isotopes of Qad-2 calcite dated at 0.005 ± 0.007 ka (calcite age between 1938 and 1952 CE) show average $\delta^{13}\text{C}$ and $\delta^{18}\text{O}$ values of -7.2‰ and -6.6‰ , respectively. On a comparative basis, present cave and spring water sampled in 2011 and 2014 in Qadisha Cave (Nehme et al., 2019) show average values of -8.6‰ for $\delta^{18}\text{O}_w$ and -46.9‰ for $\delta^2\text{H}_w$.

Average fluid inclusion $\delta^{18}\text{O}_w$ and $\delta^2\text{H}_w$ values for Qad-2 are -6.5‰ and -41.8‰ , respectively. Samples taken at approximately the same level B in the stalagmite (~ 9.0 – 9.1 ka) show a certain variability of 3.6‰ for $\delta^2\text{H}$ and 2.6‰ for $\delta^{18}\text{O}$, between samples. The sample with the highest water yield shows the most negative $\delta^{18}\text{O}$ value. At ~ 7.2 – 7.3 ka, $\delta^{18}\text{O}_w$ is -7.0‰ and $\delta^2\text{H}_w$ is -42.8‰ (Table 2). Level E, which spans the time period of the last century, yielded a very low amount of water and was therefore rejected.

High-resolution trace element data

Main trace element ratios presented in Figure 3 are all above-background levels. The overall sampling resolution is annual to multi-annual. The average elementary ratios show a slight shift between Qad-1 and Qad-2, with a higher variability for Qad-1 in general. Mg/Ca ratios show a few significant shifts that are

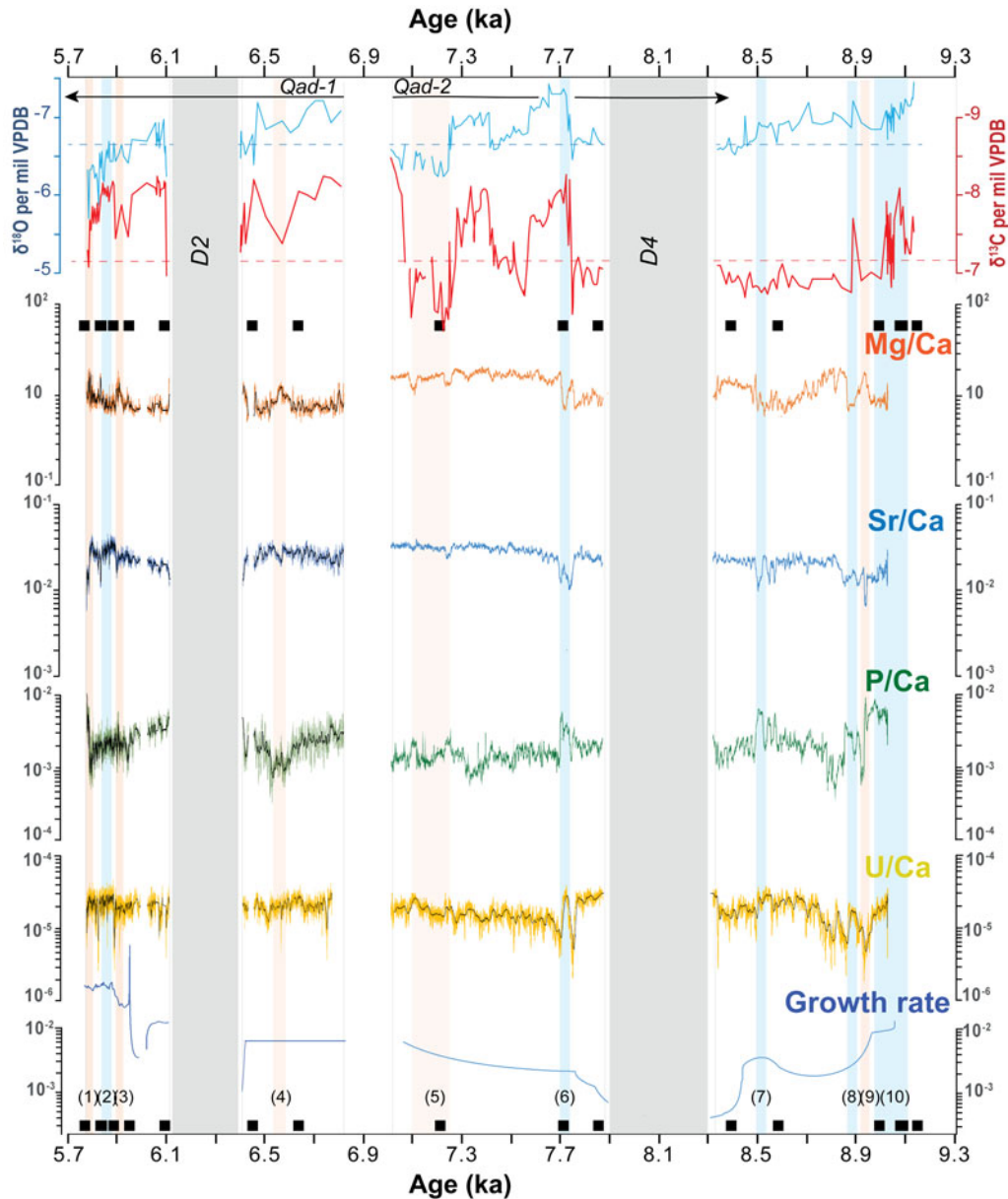


Figure 3. $\delta^{18}\text{O}$ and $\delta^{13}\text{C}$ profiles of both Qad-1 and Qad-2 stalagmites with the trace elements curves (Mg/Ca, Sr/Sa, P/Ca, U/Ca) and a moving average curve (in black) for some of the trace elements. Growth rate is displayed in logarithmic scale. Both stable isotope and trace element data are plotted against time (yr 1950 CE), modeled using StalAge. Black dots refer to the dating points and the gray shading to the identified discontinuities (D2, D4). Blue rectangles highlight significant variations toward wetter conditions in both stable isotopes and trace element data, and orange rectangles highlight drier conditions. Dashed lines crossing the $\delta^{18}\text{O}$ and $\delta^{13}\text{C}$ profiles indicate present-day values. Rapid dry and wet events are numbered from 1 to 10.

Table 2. Qadisha fluid inclusion samples in chronological order (old to young).^a

| Qad_2 samples ^b | Age of level ka 1950 CE | Sample code | δH^2 per mil | $\delta^{18}\text{O}$ per mil | Volume μl | Mass g | Water amount $\mu\text{l/g}$ | Temperature _{fi} ^c °C |
|----------------------------|-------------------------|-------------|----------------------------|-------------------------------|----------------------|--------|------------------------------|---|
| Level B | ~9.1–9.0 | BQ_2_d | –41.70 | –5.81 | 0.29 | 0.58 | 0.50 | 18.7 ± 2.5 |
| Level B | ~9.1–9.0 | BQ_2_b | –43.20 | –7.65 | 0.73 | 0.78 | 0.94 | 10.3 ± 2.5 |
| Level B* | ~9.1–9.0 | BQ_2_a | –39.58 | –5.53 | 0.23 | 0.72 | 0.32 | 20.1 ± 2.5 |
| Level A | ~7.3–7.2 | AQ_1 | –42.82 | –7.04 | 0.39 | 0.46 | 0.84 | 12.2 ± 2.3 |
| Level E* | ~0.05 | EQ_1 | –19.46 | –6.88 | 0.01 | 0.45 | 0.02 | 11.2 ± 2.4 |

^aStable isotope measurements are shown for 1 σ error.

^bMeasurements with an asterisk (*) are considered outliers due to a low water amount of less than 0.5 $\mu\text{l/g}$.

^cApparent formation temperature was determined using the calcite–water fractionation factors after Kim and O’Neil (1997).

mirrored in most other investigated ratios (Fig. 3). Particularly strong trace elemental signals are visible around ~9.0–8.9 and ~7.7 ka, whereas weaker signals are noticeable at ~8.5, ~7.3 and ~7.1, ~6.6, and ~5.8 ka.

DISCUSSION

Age-growth behavior of the studied speleothems

Both stalagmites grew during the Holocene, roughly between 9.2 and 5.7 ka, one succeeding the other, suggesting favorable (humid and warm) conditions for stalagmite deposition at the high altitude of Qadisha Cave. Although growth is relatively constant over most parts of the stalagmites, several hiatuses are observed. Former studies on stalagmites from Mt. Lebanon (Verheyden et al., 2008; Nehme et al., 2015, 2018) suggest that cave calcite precipitation, and thus growth in the central Levant, is conditioned by effective infiltration (Cheng et al., 2015). This growth cessation may be site-specific but could also reflect unfavorable conditions for calcite deposition, such as dry conditions with low effective infiltration within the epikarst or scarcer vegetation with less bio-vegetation activity. Based on the number of currently analyzed speleothems, one cannot determine which option is correct.

Growth rates of both stalagmites are of the same order, reflecting similar drip rates and cave $p\text{CO}_2$. Similarities in the petrography of both speleothems corroborate consistent growth conditions. High growth rates of 0.15–0.6 mm/yr between 6.1 and 5.8 ka and of 0.3–0.9 mm/yr between 9.15 and 9.0 ka allow for annual and higher-resolution climate reconstruction. Growth rates of 15–50 $\mu\text{m}/\text{yr}$ for most other parts of the record allow at least for multi-annual resolution using a traditional micro-milling technique for stable isotope analysis. Two growth pauses at 8.3–7.8 ka and 6.4–6.1 ka are supported by two clear petrographic discontinuities. The growth pauses between 8.3 and 7.8 ka in the Qad-2 stalagmite, although supported petrographically by a thin dust layer, are not supported by changes in other proxies before or after the hiatus. If regional aridification characterized the 8.2 ka event, as inferred from the lowland Jeita Cave record (Cheng et al., 2015), then a combination of low infiltration and scarcer vegetation within the Qadisha karst basin would make speleothem growth highly unfavorable, plausibly leading to a centennial-scale hiatus. Such a hiatus is observable in Qad-2, but cannot be attributed confidently to climatic change.

Unlike the growth stop dated between 8.3 and 7.8 ka in Qad-2, the one dated between 6.5 and 6.1 ka in Qad-1 seems to be clearly framed by changes in stable isotope values and trace elements. More positive $\delta^{18}\text{O}$ and $\delta^{13}\text{C}$ values suggest drier conditions before and directly after the growth stop and may record unfavorable growth conditions, although prior calcite precipitation related to local factors at the drip rate may occur, and other speleothems need to be studied to confirm our hypothesis. This seems also in agreement with a change toward increased Mg/Ca values and decreased Sr/Ca values just before and after the hiatus.

Interpreting the changes in geochemical proxies from Qadisha Cave

Speleothem $\delta^{18}\text{O}$ and $\delta^{13}\text{C}$

In the Levant, it is now widely established that the $\delta^{18}\text{O}$ signal is interpreted as related to effective recharge in the epikarst (precipitation amount vs. evapotranspiration), and therefore indicates water balance (P-E) in the epikarst (Bar-Matthews et al., 2003;

Verheyden et al., 2008; Cheng et al., 2015; Nehme et al., 2020). Higher infiltration (more positive P-E) is related to pronounced low-pressure systems with significant rainfall. Higher rainfall amounts are known to cause more negative rainfall $\delta^{18}\text{O}$ values (Bar-Matthews et al., 2003; Aouad-Rizk et al., 2005), and reduced annual rainfall (with concomitant reduced P-E) produces higher rainfall $\delta^{18}\text{O}$ values.

At mid-latitudes, $\delta^{13}\text{C}$ and growth rate in speleothems are related to biological CO_2 production, which is dependent on soil and vegetation conditions in the catchment (Genty et al., 2001a, 2001b). Warmer and wetter periods usually enhance the production of biogenic, $\delta^{13}\text{C}$ -depleted CO_2 and increase the growth rate (Genty et al., 2001a, 2001b). Cold/dry conditions reduce the vegetation cover and the biogenic CO_2 supply. Lower/higher calcite $\delta^{13}\text{C}$ values and faster/slower growth rates are therefore usually indicative of soil development/disruptions and can be related to warmer-wetter/colder-drier conditions. An additional control on $\delta^{13}\text{C}$ is exerted by the hydrologic state of the aquifer. Partial dewatering of the drip-feeding system induces longer residence times and prior calcite precipitation, leading to higher $\delta^{13}\text{C}$ during drier periods (Fairchild and Baker, 2012).

The stable isotopic $\delta^{18}\text{O}$ values of both Qadisha stalagmites display a general trend toward more positive $\delta^{18}\text{O}$ values from 8.5 to 5 ka. This general $\delta^{18}\text{O}$ trend comprises three independent segments that include several rapid shifts toward negative values at ~9.1 ka (10), ~8.9 ka (8), ~8.5 ka (7), ~7.7 ka (6), and 5.8 ka (2) (see Fig. 3 for numbers in parentheses). Such negative “peaks” are interpreted as wet intervals with high effective recharge (high growth intervals of the stalagmites) and a positive water balance (P-E) (Cheng et al., 2015). Rapid changes toward more positive $\delta^{18}\text{O}$ at ~9.0 ka (9), ~7.2–7.1 ka (5), ~6.6 ka (4), ~5.9 ka (3), and ~5.7 ka (1), are particularly well expressed and chronologically constrained. Some of these periods interpreted here as “drying” events, particularly at ~9.0 (9), are characterized by unusually high growth rates. Such peculiar periods seem to indicate, at least locally, a wet period, as confirmed by negative (lower) $\delta^{13}\text{C}$ values, before the short dry period of ~80 yr, but still with high growth rates. Albeit with low resolved growth rates compared with the resolution of geochemical proxies (annual for trace elements and decadal for the $\delta^{13}\text{C}/\delta^{18}\text{O}$), such peculiar drying events preceded by short wet events reflect a rapid decadal variability, inferring a shift in the distribution of effective infiltration.

Trace elements

In general, the (trace) element concentrations of Mg, Sr, P, and U in calcite are controlled by hydrologic processes and less by cave temperature (Roberts et al., 1998). Speleothem Sr/Ca ratios constitute a sensitive proxy for infiltration changes in the epikarst, with higher values being recorded during times of reduced effective moisture availability (Fairchild and Treble, 2009). Other mechanisms can explain Sr mobility within the epikarst and include changes in weathering rates, aerosol input, and soil activity that can induce high-frequency variability on short timescales (decadal to annual) (Verheyden et al., 2000; Fairchild et al., 2006; Sinclair et al., 2012; Baker et al., 2021). For Mg/Ca ratios in speleothems, it is common to attribute an increase to a response to PCP during times periods of low effective infiltration (Verheyden et al., 2000; Tooth and Fairchild, 2003; McDermott, 2004; Fairchild et al., 2006). Because Sr/Ca ratios are similarly influenced by PCP, Mg and Sr ratios are often positively correlated.

An exception to this behavior occurs in the presence of dolomitized limestone in the karst aquifer, as is the case in the Qadisha basin, where processes of incongruent calcite dissolution and/or differentiated soil input may play a role (Roberts et al., 1998; Hellstrom and McCulloch, 2000; Huang et al., 2001; Sinclair et al., 2012; Jamieson et al., 2016).

Phosphorous and U are less commonly studied but increasingly used as proxies in the speleothem archive. This element is generally mobilized from soils during early autumnal/winter storms. High P/Ca in speleothems reflects maximum soil infiltration during heavy rainfalls at the start of wet seasons (Borsato et al., 2007). The P/Ca ratio can be complemented by other paleo-hydrologic proxies such as Ba/Ca or U/Ca. Uranium is generally leached from the bedrock during high-rainfall events and results in high U/Ca in the calcite. (Ayalon et al., 1999; Treble et al., 2003; Fairchild and Treble, 2009)

In the Qadisha speleothems, the trace element concentrations vary at maximum by two orders of magnitude. Wet and dry episodes identified by stable isotopes and growth rate changes (section 7.2.a, Fig. 3) can overall be linked to changes in the trace element concentrations, with generally high Mg/Ca, and low Sr/Ca, P/Ca, and U/Ca corresponding to higher stable isotope values, suggesting an overall common driver, although with different sensitivities between proxies. Therefore, in the Qadisha speleothems, we assign the periods with high $\delta^{13}\text{C}/\delta^{18}\text{O}$ and Mg (and generally low Sr, P, and U) to dry periods, with a lower water recharge in the epikarst, and the opposite changes to wet periods. At 9.0 ka and 7.7 ka, significant changes in $\delta^{13}\text{C}$ and $\delta^{18}\text{O}$ values, as well as in U and P concentrations, may suggest the occurrence of important flushing episodes.

Infiltration water isotopes based on fluid inclusion analysis

Isotope measurements of fluid inclusion water (δD ; $\delta^{18}\text{O}_w$) can provide insights into the hydrologic cycle and allow estimation of mineral formation temperatures. Three successful fluid inclusion analyses from the Qad-2 stalagmite with water amounts $>0.5 \mu\text{l/g}$ were retained here (Table 2). The $\delta^{18}\text{O}$ and δD values of water sampled in pools, cave streams, and drip water inside Qadisha Cave vary between -8.4 and -9.0 and between -45.7‰ and -49.5‰ , respectively. The d-excess of the cave water is between 21.4‰ and 22.6‰ (Nehme et al., 2019). As the cave water represents an average of the annual precipitation, rainfall values in contrast show a higher variability from -12.6‰ to $+1.2\text{‰}$ and -86‰ to $+11.6\text{‰}$ for $\delta^{18}\text{O}$ and δD values, respectively (Aouad-Rizk et al., 2005). The d-excess values are between 2‰ and 27‰ , with an average close to that of the cave water (Aouad-Rizk et al., 2005), indicating a generally higher d-excess for Lebanon compared with the global meteoric water line. Although fluid inclusions (FI) values fall within the modern-day range of rain water, compared with modern-day drip water from Qadisha, they show important variability. Especially, the samples from the B-level (9.0–9.1 ka) raise questions about the lateral coherency of the isotopic composition of FI water. The variability between different levels (B vs. E) may be related to differences in isotopic composition of the rain and therefore the fluid inclusions. Overall, the results are more positive than today's drip water isotopic composition. Following our interpretation, these values dated within the intervals of 7.3–7.2 ka and 9.1–9.0 ka represent isotopic values of water precipitated close to dry events (5) and (9) identified based on their more positive calcite $\delta^{13}\text{C}$ and $\delta^{18}\text{O}$ values (Fig. 4) and may suggest short-term drier

conditions in the generally wetter Early to Middle Holocene. A higher fraction of summer rainfall contribution to the water budget with a higher isotope value compared with winter snow with its lower isotopic composition (Aouad-Rizk et al., 2005) may be another possible explanation for this isotopic observation. In Soreq Cave, Early to Middle Holocene fluid inclusion isotope values are comparable or slightly more negative compared with modern-day values (Matthews et al., 2021). This contrasting effect could be related to Sapropel S1, which has a significant effect on the isotope values in the southern Levant (Bar-Matthews et al., 2003) but is not particularly expressed in the northern Levant (e.g., the Jeita record; Cheng et al., 2015), where rainfall amounts are generally higher. In addition, snowfall is of minor importance for the infiltration budget at Soreq Cave, whereas it is today the dominant water source in the region around Qadisha Cave.

The fluid inclusion isotope values of various Early to Middle Holocene speleothems along the Levant become more negative from south (Soreq Cave) to north (Qadisha Cave), in agreement with a dominating altitudinal effect and, in addition, an increase in average rainfall toward the Lebanon mountains (Nehme et al., 2019). The difference in drip-water $\delta^{18}\text{O}$ values between Soreq and Qadisha Caves is $\sim 4\text{‰}$, which is close to the expected difference from altitude alone. The elevation difference is about 1400 m, which explains an isotopic shift of $2.8\text{--}4.2\text{‰}$ at a lapse rate of $0.2\text{--}0.3\text{‰}/100 \text{ m}$ (Clark and Fritz, 1997). The difference between measured fluid inclusion isotope values of Holocene samples from the Soreq and Qadisha Caves is similar. Although hardly resolvable with the current set of fluid inclusion data, rainfall amount could also play a role. For example, Mizpe Shelagim is situated at almost the same elevation as Qadisha Cave, but about 120 km to the south, and shows a more positive $\delta^2\text{H}$ value than Qad-2.

The climatic conditions during the Holocene optimum

Global and regional drivers of climatic variability during the Holocene optimum

The Qadisha stalagmites grew from 9.2 to 5.7 ka, albeit with a discontinuous trend, and show a general tendency from more negative $\delta^{18}\text{O}$ values during the Early Holocene toward more positive $\delta^{18}\text{O}$ values at the end of the Holocene optimum. This trend reflects a change from a wetter (more positive P-E) toward a drier climate (reduced P-E) in this high-altitude area. This trend is also noticeable at low altitude; for example, in the Jeita $\delta^{18}\text{O}$ record and in other speleothem records from the southern Levant (e.g., Mizpe Shelagim and Soreq Caves) (Fig. 5A). The carbon signal in Qadisha indicates values reaching -8‰ during wet peaks and shifts to -6‰ during dry events (Fig. 5B), reflecting higher soil and vegetation activity during humid periods. The $\delta^{13}\text{C}$ curve overprints the short-term changes with a slow long-term increasing trend (Fig. 5B) toward more negative values when reaching the mid-Holocene, suggesting overall improved bio-pedological soil activity in the Makmel mountains from 9 to 6 ka.

The two investigated Qadisha stalagmites started to grow during the period of maximum summer insolation (Berger and Loutre, 1991) and a high sea-surface temperature (SST) in the EM, reaching $\sim 18^\circ\text{C}$ during the Holocene optimum (Fig. 6) (Emeis et al., 2003; Scrivner et al., 2004). From 10 to 6.5 ka, the deposition of Sapropel 1 in the EM occurred as a result of increased discharge of the river Nile, leading to isotopically lighter sea-surface water. The contribution of the Mediterranean source

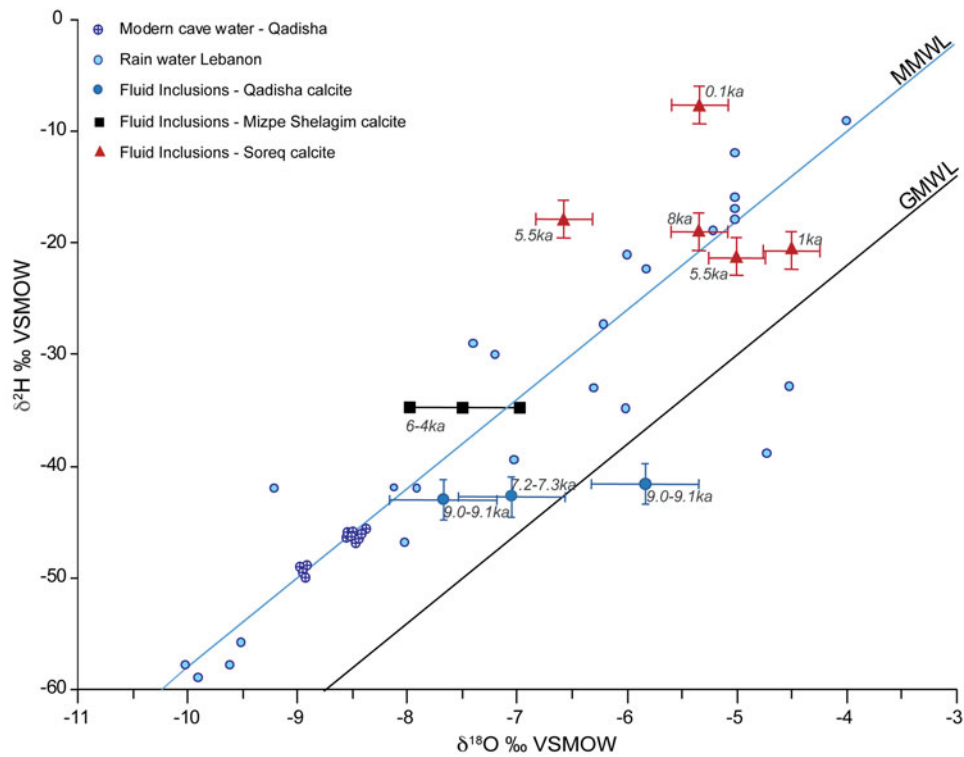


Figure 4. Graph showing the fluid inclusion stable isotopes of the Qadisha stalagmite (this study) in comparison with fluid inclusions (FI) from the Mizpe Shelagim (Ayalon et al., 2013) and Soreq records (Matthews et al., 2021), all plotted against the global (GMWL; Rozanski et al., 1993) and Mediterranean meteoric water lines (MMWL; Gat et al., 2003). Modern rain water in Lebanon (Aouad-Rizk et al., 2005; Saad et al., 2005) is plotted in blue circles; modern cave water of Qadisha Cave is plotted in hatched circles.

effect as the only factor in the $\delta^{18}\text{O}$ -depleted signals in terrestrial records has been debated in the last decades. Recent studies on Yammounh lake (Develle et al., 2010) and the Soreq (Grant et al., 2016) and Zalmon Caves (Keinan et al., 2019) show a

contribution of rainfall amount in changes of the $\delta^{18}\text{O}$ signal throughout glacial–interglacial cycles and even during the sapropel events, by extracting the source signal (the $\delta^{18}\text{O}_{\text{g.rubber}}$) from the $\delta^{18}\text{O}_{\text{calcite}}$ of speleothems or $\delta^{18}\text{O}_{\text{ostrac}}$ signal of lake ostracods.

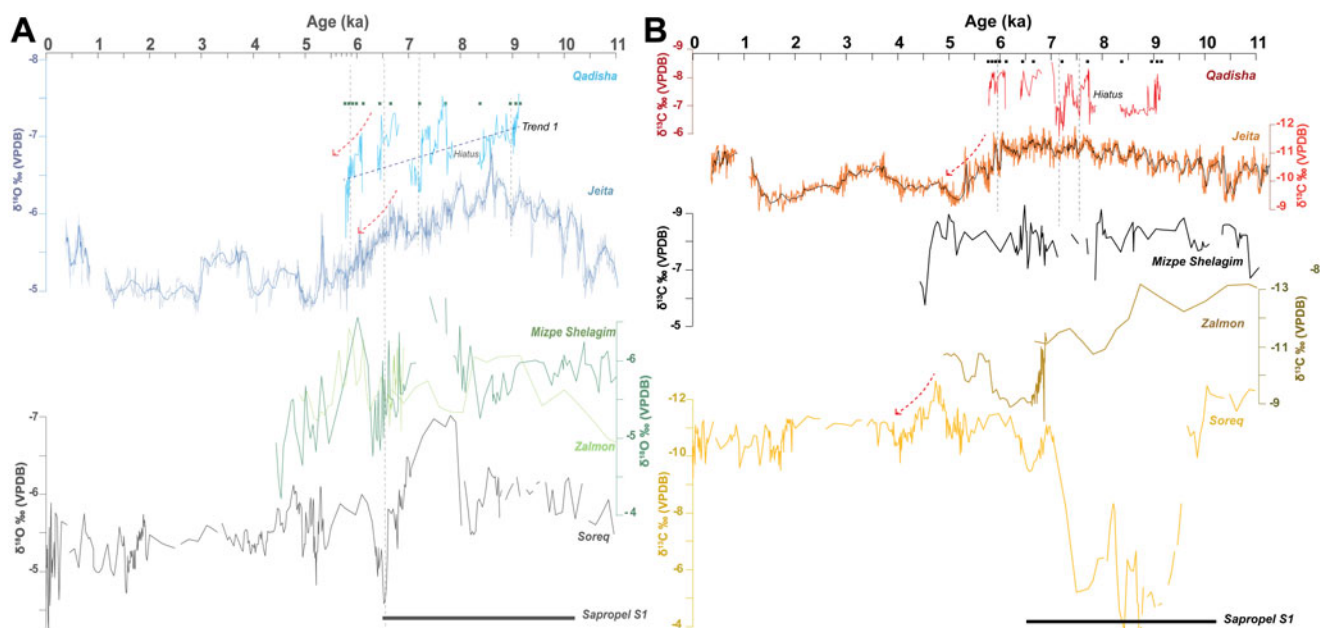


Figure 5. Plots of the Qadisha stable isotope curve in comparison with other speleothem records in the Levant. (A) Carbon isotope curves; (B) oxygen isotope curves. Black dots represent U-Th dating points in the Qadisha record.

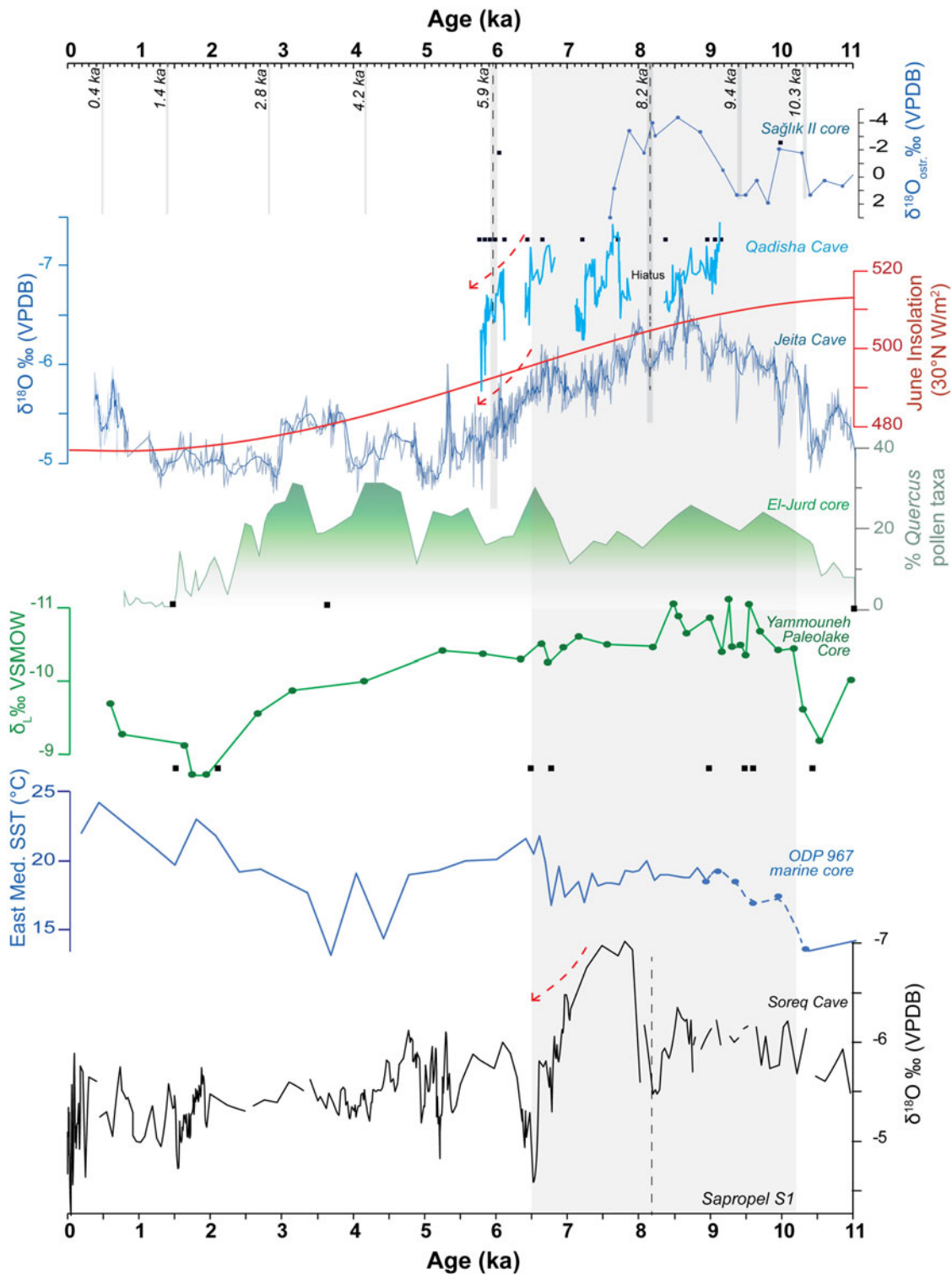


Figure 6. Comparison of the Qadisha record with regional records in the eastern Mediterranean (EM) region. From top to bottom: Sağlık II $\delta^{18}\text{O}_{\text{ostracods}}$, Turkey (Sekeryapan et al., 2020), Qadisha $\delta^{18}\text{O}_c$ record, Lebanon (this study) Jeita $\delta^{18}\text{O}_c$ record, Lebanon (Cheng et al., 2015), the Summer Insolation curve (Berger and Loutre, 1991), *Quercus* pollen taxa percentage from El-Jurd core (Cheddadi and Khater, 2016), $\delta^{18}\text{O}_l$ Yammouneh record (Develle et al. 2010), EM sea-surface temperature (SST), ODP 967 (Emeis et al., 2003; Scrivner et al., 2004), Soreq $\delta^{18}\text{O}_c$ record (Bar-Matthews et al., 2003)

An increased precipitation over Mt. Lebanon during the Sapropel 1 event is noticeable with depleted $\delta^{18}\text{O}_{\text{lake}}$ (corrected from the source) signal reaching -11% in Yammouneh lake, from 9.2 to 8.3 ka. Likewise, the uncorrected $\delta^{18}\text{O}_{\text{ostrac.}}$ signal of the lowland

Sağlık II peat record (Sekeryapan et al., 2020) in the northern part of the Levant, albeit a low-resolved curve, reach the most depleted ostracod $\delta^{18}\text{O}$ values between 9 and 7.7 ka. The well-dated lowland Jeita Cave record in central Lebanon shows the

most-depleted values for the whole record around 8.5 ka, followed by a sharp $\delta^{18}\text{O}$ drop (less negative values) from 8.5 to 8 ka and then a general decrease with less negative $\delta^{18}\text{O}$ values until 5 ka.

More locally, in the Makmel Mountains, the *Quercus* pollen taxa in the Al-Jurd peat core (Cheddadi and Khater, 2016), located 23 km north of Qadisha Cave, show a relatively high pollen percentage from 10 to 8 ka, followed by a reduced *Quercus* pollen percentage from 8 to 6.5 ka, and marked later by an increase of *Quercus* pollen percentage at 6.5, 5.5, 4.5, and 3 ka (Fig. 6). Albeit a low-resolved curve, the pollen record of the Al-Jurd peat core seems to show a higher percentage of *Quercus* pollen during the mid-Holocene (6.5 to 3 ka) rather than in the Early Holocene period from 9 to 6 ka, as indicated by several speleothems. The *Quercus* forest extension after 6.5 ka is rather puzzling in the local paleoclimate scheme (speleothems) of the Makmel mountains, but could suggest wetter/warmer conditions with improved bio-pedogenic activity in soils coeval with a reduced snow season and/or decreased snow cover enabling the extension of the forest. During the Early Holocene, slightly colder/drier conditions (than during the mid-Holocene) might have prevailed, with the persistence of a longer snow cover period impacting the length of the plant growing season but enhancing speleothem growth with an important recharge from the during summer. Soil erosion is enhanced during short melt seasons on the long-term trend in the Makmel Mountains and would explain the reduced *Quercus* forest in the area. In a similar alpine context such as in the Rio Martino Cave, Piedmont Alps, Italy (Regattieri et al., 2019), it was suggested that an increase in the persistence of snow cover may also impact the $\delta^{13}\text{C}$ by reducing the length of the plant growing season, leading to reduced biogenic CO_2 supply and therefore to a less negative $\delta^{13}\text{C}$ signal in speleothems. Above the Qadisha site, the cedar forest stretching over same altitude as the El-Jurd site may have had similar reduction/extension dynamics during the Early/Middle Holocene, thus leading in general from $\delta^{13}\text{C}$ signal (avg: -7‰) in Qadisha speleothems in the Early Holocene to a slightly more negative $\delta^{13}\text{C}$ signal (avg: -8‰) in the mid-Holocene.

Centennial-scale climate variability

Rapid climatic changes at the centennial scale are recorded in some of the highly resolved stalagmites along the Levantine coast. Cheng et al. (2015) detected nine cold/dry events in the Jeita record during the Holocene coeval with those in the North Atlantic sediments (Bond et al., 2001). The Bond events in the Jeita record are interpreted as dry events inferred from both $\delta^{18}\text{O}$ and $\delta^{13}\text{C}$ variations (Cheng et al., 2015) (Figs. 5 and 6). Some of the events, such as the ~ 5.1 ka event, noticeable in the Jeita record, is also recorded as a dry event in Anatolian lake records (Roberts et al., 2011). The 8.2 ka event recorded in the Jeita stalagmite corresponds to a $\delta^{18}\text{O}$ and $\delta^{13}\text{C}$ excursion (Fig. 4) in Soreq Cave (Bar-Matthews et al., 2003). Such an event is, however, not noticeable in other speleothem records along the Levantine coast or in Yammounh lake (Develle et al., 2010). In Qadisha Cave, the 8.2 ka cold event is not expressed or may be related to the growth stop.

Other events, at ~ 8.9 – 9.0 ka, ~ 7.1 ka, and ~ 5.9 ka (Fig. 4) in the Jeita record are also visible in the Qadisha record, with more positive stable isotope values (dry events) but with less-clear changes in the related trace element pattern. In contrast, RCC interpreted as wet events in Qadisha Cave, such as the most prominent 7.7 ka wet period, are not noticeable in the Jeita record but correspond to the major peak in the Soreq record (Fig. 5A).

The inconsistency in recording rapid climate change events between Levantine records may be due to different proxy resolution (e.g., smoothing in case of too low resolution) or differences in the local archive sensitivity to RCC.

Altitudinal and snow cover effect on the significance of climate signals

In the Levant, most of the published speleothem records are located at low altitudes facing the Mediterranean Sea, except for the Incesu and Mizpe Shelagim records located at 1615 m and 2180 m, respectively. Only at Mizpe Shelagim a plausible link between the effect of snow cover at high altitudes and speleothem growth was established on glacial–interglacial timescales. During the Holocene interglaciation, the snow cover in mountain areas participated actively in the epikarst water budget, fed drip sites, and favored speleothem growth in caves located at high altitudes, as well as affecting the vegetation dynamics. Whereas temperature remains close to 0°C during winter over large areas of Mt. Lebanon (Fayad and Gascoïn, 2020), the soil beneath the snow does not freeze under present winter conditions, except during exceptional cold events. Comparison of the Qadisha records with those located at low altitudes helps in deciphering altitudinal trend and local particularities.

The Qadisha stalagmites show more negative $\delta^{18}\text{O}$ values (Fig. 5A) than those recorded by the Jeita stalagmite related to the altitudinal effect expressed in the rain and cave water isotopic signals (Nehme et al., 2019). Also, the contribution of snow to the infiltration and the percolation water in caves (Aouad-Rizk et al., 2005) may lead to more negative drip-water and calcite $\delta^{18}\text{O}$ values. It is noteworthy that the Qadisha stalagmites display a larger amplitude in the $\delta^{18}\text{O}$ changes and therefore have a more dynamic response to changes than the Jeita record. This behavior may be related to the higher altitude and the enhanced convective rainout at mountain ranges as well as to the generally lower $\delta^{18}\text{O}$ values of snow. An increase in low-pressure systems can disproportionately increase the rainfall/snow amount in high-altitude mountain regions. Qadisha records can therefore better, or at least more clearly, indicate RCC than the low-elevation Jeita speleothems. In contrast, short-term dry conditions may be better recorded by the lower-elevation archive sites, as they are more sensitive to droughts and PCP, which enhances the isotope and element signal. An example is the drought event recorded in Soreq, Mizpe Shelagim, and Zalmon Caves around 6.5 ka, which is well expressed in these caves, but less well expressed in Qadisha Cave.

More to the south, the Zalmon and Soreq records indicate changes in the $\delta^{13}\text{C}$ values of more than 4‰ throughout the Holocene (Fig. 5B). This drastic shift in the $\delta^{13}\text{C}$ signal of Zalmon Cave is mirrored by the $\delta^{13}\text{C}$ signals in other records, with a trend toward less negative $\delta^{13}\text{C}$ values by the end of the Holocene optimum. Although marked by a high $\delta^{13}\text{C}$ shift, the vegetation in northern Galilee indicates a reduced bio-pedological activity after 8.5 ka, whereas the soil activity seems to be less variable throughout the Holocene optimum at the Jeita coastal site until 6 ka. In the case of Qadisha Cave, the carbon isotope signal reflects a higher sensitivity of the vegetation to humidity changes with step changes ($< 2\text{‰}$), similar to Mizpe Shelagim (Mt. Hermon). In Soreq Cave located to the south, the shift to less negative carbon values that are closer to the bedrock signal throughout the Holocene optimum, is interpreted as reflecting a soil denudation by intensive storms. The vegetation cover appears to be more stable at Jeita and changes drastically only during

larger climatic shifts (e.g., 6 ka), whereas the soil system at high-altitude sites (Qadisha and Mizpe Shelagim) is more sensitive to rapid changes in the water budget and the snow cover dynamics and indicates short-term erosional phases between 7 and 6 ka.

CONCLUSIONS

New stalagmites from Qadisha Cave (Lebanon) located in the high Mt. Makmel, north of Mt. Lebanon, provide a well-dated record for the northern Levant with high-resolution geochemical proxies ($\delta^{18}\text{O}$ and $\delta^{13}\text{C}$ values, trace element concentrations). The Qadisha stalagmites grew from 9.2 to 5.7 ka, albeit with discontinuities, and show a general tendency from more negative $\delta^{18}\text{O}$ values during the Early Holocene toward more positive $\delta^{18}\text{O}$ values at the end of the Holocene optimum. This trend is in agreement with a change from a wetter to a drier climate in this high-altitude area. The $\delta^{13}\text{C}$ values show rapid shifts along the record and a decreasing trend toward more negative values when reaching the mid-Holocene. The slight trend toward more negative values suggests overall improved bio-pedological soil activity in the Makmel Mountains during the mid-Holocene. Discrepancies between pollen data showing a wetter period at 7–6 ka than at 7–9 ka, unlike speleothems showing an overall wet Early Holocene, are interpreted as related to a reduced snow cover season and thickness since 6.5 ka, explaining the extension of *Quercus* at 6.5 ka. On the short-term climate trend, Qadisha stalagmites record rapid dry and wet changes on a centennial scale from 9 to 5 ka, with a tendency for drier conditions toward the mid-Holocene.

The Qadisha record is in good agreement with other Levantine records, such as the one from Jeita Cave, showing overall more humid climatic conditions from 9 to 7 ka in the region. After 7 ka, a drier climate seems to affect sites in both low- and high-altitude areas. The Qadisha record reflects particularities of a mountainous climate compared with other records: (1) more negative stable isotope values than the Jeita record due to the altitudinal rainout effect; (2) a larger amplitude in the oxygen isotopes, reflecting a more dynamic response to RCC than records located at lower altitudes; and (3) the effect of snow cover and duration regulating the effective infiltration in the Makmel area.

Acknowledgments. This study and field mission was funded by the 2014 mobility fellowship program of the Belgian Federal Scientific Policy (BELSPO). We acknowledge the assistance of Saint-Joseph University of Beirut for facilitating the access to caves with the help of ALES (Association Libanaise d'Etudes Spéléologiques) and SCL (Spéléo-Club du Liban) and the support of members of both caving clubs who collected water and calcite samples during field campaigns. Fluid inclusion measurements were supported by grant DFG KL2391/2-1 and uranium/thorium dating was funded by NSF grant 2202913 to RLE.

REFERENCES

Affolter, S., Fleitmann, D., Leuenberger, M., 2014. New on-line method for water isotope analysis of speleothem fluid inclusions using laser absorption spectroscopy (WS-CRDS). *Climate of the Past* **10**, 1291e1304.

Almogi-Labin, A., Bar-Matthews, M., Shriki, D., Kolosovsky, E., Paterne, M., Schilman, B., Ayalon, A., Matthews, A., 2009. Climatic variability during the last ~90 ka of the S. and N. Levantine Basin as evident from marine records and speleothems. *Quaternary Science Reviews* **28**, 2882–2896.

Alpert, P., Price, C., Krichak, S.O., Ziv, B., Saaroni, H., Osetinsky, I., Kishcha, P., 2005. Tropical teleconnections to the Mediterranean climate and weather. *Advances in Geosciences* **2**, 157–160.

Aouad-Rizk, A., Job, J.O., Khalil, S., Touma, T., Bitar, C., Bocquillon, C., Najem, W., 2005. $\delta^{18}\text{O}$ and $\delta^2\text{H}$ contents over Mt. Lebanon related to mass trajectories and local parameters. In: *Isotopic Composition of Precipitation in the Mediterranean Basin in Relation to Air Circulation Patterns and Climate*. IAEA-TECDOC 1453. Vienna: International Atomic Energy Agency, pp. 75–82.

Ayalon, A., Bar-Matthews, M., Frumkin, A., Matthews, A., 2013. Last glacial warm events on Mt. Hermon: the southern extension of the Alpine karst range in the east Mediterranean. *Quaternary Science Reviews* **59**, 43–56.

Ayalon, A., Bar-Matthews, M., Kaufman, A., 1999. Petrography, strontium, barium and uranium concentrations, and strontium and uranium isotope ratios in speleothems as palaeoclimatic proxies: Soreq Cave, Israel. *Holocene* **9**, 715–722.

Ayalon, A., Bar-Matthews, M., Sass, E., 1998. Rainfall-recharge relationships within a karstic terrain in the Eastern Mediterranean semi-arid region, Israel: $\delta^{18}\text{O}$ and $\delta^2\text{H}$ characteristics. *Journal of Hydrology* **207**, 18–31.

Ayalon, A., Bar-Matthews, M., Schilman, B., 2004. *Rainfall Isotopic Characteristics in Various Sites in Israel and the Relationships with the Unsaturated Zone Water*. Israel Geological Survey Report GSI/16/04. Geological Survey of Israel, Jerusalem.

Baker, A., Mariethoz, G., Comas-Bru, L., Hartmann, A., Frisia, S., Borsato, A., Asrat, A., 2021. The properties of annually laminated stalagmites—a global synthesis. *Reviews of Geophysics* **59**(2), e2020RG000722.

Bar-Matthews, M., Ayalon, A., 2011. Mid-Holocene climate variations revealed by high-resolution speleothem records from Soreq Cave, Israel and their correlation with cultural changes. *Holocene* **21**, 163–171.

Bar-Matthews, M., Ayalon, A., Gilmour, M., Matthews, M., Hawkesworth, C., 2003. Sea-land isotopic relationships from planktonic foraminifera and speleothems in the Eastern Mediterranean region and their implications for paleorainfall during interglacial interval. *Geochimica et Cosmochimica Acta* **67**, 3181–3199.

Bar-Matthews, M., Ayalon, A., Matthews, A., Sass, E., Halicz, L., 1996. Carbon and oxygen isotope study of the active water-carbonate system in a karstic Mediterranean cave: implications for paleoclimate research in semi-arid regions. *Geochimica et Cosmochimica Acta* **60**, 337–347.

Berger, A., Loutre, M.F., 1991. Insolation values for the climate of the last 10 million years. *Quaternary Science Reviews* **10**, 297–317.

Berrisford, P., Källberg, P., Kobayashi, S., Dee, D., Uppala, S., Simmons, A.J., Poli, P., 2011. Atmospheric conservation properties in ERA-Interim. *Quarterly Journal of the Royal Meteorological Society* **137**, 1381–1399.

Bond, G., Kromer, B., Beer, J., Muscheler, R., Evans, M.N., Showers, W., Hoffmann, S., Lotti-Bond, R., Hajdas, I., Bonani, G., 2001. Persistent solar influence on North Atlantic climate during the Holocene. *Science* **294**, 2130–2136.

Borsato, A., Frisia, S., Fairchild, I.J., Somogyi, A., Susini, J., 2007. Trace element distribution in annual stalagmite laminae mapped by micrometer-resolution X-ray fluorescence: implications for incorporation of environmentally significant species. *Geochimica et Cosmochimica Acta* **71**, 1494–1512.

Brayshaw, D.J., Rambeau, C.M., Smith, S.J., 2011. Changes in Mediterranean climate during the Holocene: insights from global and regional climate modelling. *Holocene* **21**, 15–31.

Burstyn, Y., Martrat, B., Lopez, J.F., Iriarte, E., Jacobson, M.J., Lone, M.A., Deininger, M., 2019. Speleothems from the Middle East: an example of water limited environments in the SISAL database. *Quaternary* **2**, 16.

Burstyn, Y., Shaar, R., Keinan, J., Ebert, Y., Ayalon, A., Bar-Matthews, M., Feinberg, J.M., 2022. Holocene wet episodes recorded by magnetic minerals in stalagmites from Soreq Cave, Israel. *Geology* **50**, 284–288.

Carolin, S.A., Walker, R.T., Day, C.C., Ersek, V., Sloan, R.A., Dee, M.W., Talebian, M., Henderson, G.M., 2019. Precise timing of abrupt increase in dust activity in the EM coincident with 4.2ka social change. *Proceedings of the National Academy of Sciences USA* **116**, 67–72.

Cheddadi, R., Khater, C., 2016. Climate change since the last glacial period in Lebanon and the persistence of Mediterranean species. *Quaternary Science Reviews* **150**, 146–157.

Cheng, H., Edwards, R.L., Shen, C.C., Polyak, V.J., Asmerom, Y., Woodhead, J., Hellstrom, J., et al., 2013. Improvements in 230Th dating, 230Th and 234U half-life values, and U–Th isotopic measurements by

- multi-collector inductively coupled plasma mass spectrometry. *Earth and Planetary Science Letters* 371, 82–91.
- Cheng, H., Sinha, A., Verheyden, S., Nader, F.H., Li, X.L., Zhang, P.Z., Yin, J.J., *et al.*, 2015. The climate variability in northern Levant over the past 20,000 years. *Geophysical Research Letters* 42, 8641–8650.
- Cheng, H., Zhang, P.Z., Spötl, C., Edwards, R.L., Cai, Y.J., Zhang, D.Z., Sang, W.C., Tan, M., An, Z.S., 2012. The climatic cyclicality in semiarid-arid central Asia over the past 500,000 years. *Geophysical Research Letters* 39, L01705.
- Clark, I. D., Fritz, P. 1997. *Environmental Isotopes in Hydrogeology*. CRC Press, Boca Raton, FL.
- Daëron, M., Drysdale, R.N., Peral, M., Huyghe, D., Blamart, D., Coplen, T.B., Zanchetta, G., 2019. Most Earth-surface calcites precipitate out of isotopic equilibrium. *Nature Communications* 10, 1–7.
- Dansgaard, W., 1964. Stable isotopes in precipitation. *Tellus* 16, 436–468.
- Demeny, A., Kele, S., Siklosy, Z., 2010. Empirical equations for the temperature dependence of calcite-water oxygen isotope fractionation from 10 to 70 °C. *Rapid Communications in Mass Spectrometry* 24, 3521–3526.
- Develle, A.L., Herreros, J., Vidal, L., Surssock, A. Gasse, F., 2010. Controlling factors on a paleo-lake oxygen isotope record (Yammoûneh, Lebanon) since the Last Glacial Maximum. *Quaternary Science Reviews* 29, 865–886.
- Dubertret, L., 1975. Introduction à la carte géologique au 50.000° du Liban. *Notes et Mémoires sur le Moyen-Orient* 23, 345–403.
- Edgell, H.S., 1997. Karst and hydrogeology of Lebanon. *Carbonates Evaporites* 12, 220–235.
- Edwards, R.L., Chen, J.H., Ku, T.L., Wasserburg, G.J., 1987. Precise timing of the last interglacial period from mass spectrometric determination of ²³⁰Th in corals. *Science* 236, 1547–1553.
- Emeis, K.C., Schulz, H., Struck, U., Rossignol-Strick, M., Erlenkeuser, H., Howell, M.W., Kroon, D., *et al.*, 2003. Eastern Mediterranean surface water temperatures and ¹⁸O during deposition of sapropels in the late Quaternary. *Paleoceanography* 18, 1005–1029.
- Erkan, G., Bayari, C.S., Fleitmann, D., Cheng, H., Edwards, L., Özbakir, M., 2022. Late Pleistocene–Holocene climatic implications of high-resolution stable isotope profiles of a speleothem from S. Central Anatolia, Turkey. *Journal of Quaternary Science* 37, 503–515.
- Fairchild, I.J., Baker, A., 2012. *Speleothem Science—From Process to Past Environments*. Blackwell Quaternary Geoscience Series. Hoboken, NJ: Wiley-Blackwell.
- Fairchild, I.J., Smith, C.L., Baker, A., Fuller, L., Spötl, C., Matthey, D., McDermott, F., 2006. Modification and preservation of environmental signals in speleothems. *Earth-Science Reviews* 75, 105–153.
- Fairchild, I.J., Treble, P.C., 2009. Trace elements in speleothems as recorders of environmental change. *Quaternary Science Reviews* 28, 449–468.
- Fayad, A., Gascoïn, S., 2020. The role of liquid water percolation representation in estimating snow water equivalent in a Mediterranean mountain region (Mt. Lebanon). *Hydrology and Earth System Sciences* 24, 1527–1542.
- Finné, M., Holmgren, K., Sundqvist, H.S., Weiberg, E., Lindblom, M., 2011. Climate in the eastern Mediterranean, and adjacent regions, during the past 6000 years—a review. *Journal of Archaeological Science* 38, 3153–3173.
- Flohr, P., Fleitmann, D., Zorita, E., Sadekov, A., Cheng, H., Bosomworth, M., Edwards, R.L., Matthews, W., Matthews, R., 2017. Late Holocene droughts in the Fertile Crescent recorded in a speleothem from N. Iraq. *Geophysical Research Letters* 44, 1528–1536.
- Fohlmeister, J., Voarintsoa, N. R. G., Lechleitner, F. A., Boyd, M., Brandtstätter, S., Jacobson, M. J., Oster, J.L., 2020. Main controls on the stable carbon isotope composition of speleothems. *Geochimica et Cosmochimica Acta*, 279, 67–87.
- Frumkin, A., Ford, D.C., Schwarcz, H., 2000. Paleoclimate and vegetation of the Last Glacial cycles in Jerusalem from a speleothem record. *Global Biogeochemical Cycles* 14, 863–870.
- Gasse, F., Vidal, L., Van Campo, E., Demory, F., Develle, A.-L., Tachikawa, K., Elias, A., *et al.*, 2015. Hydroclimatic changes in northern Levant over the past 400,000 years. *Quaternary Science Reviews* 111, 1–8.
- Gat, J.R., Klein, B., Kushnir, Y., Roether, W., Wernli, H., Yam, R., Shemesh, A., 2003. Isotope composition of air moisture over the Mediterranean Sea: an index of the air–sea interaction pattern. *Tellus*, series B 55, 953–965.
- Genty, D., Baker, A., Massault, M., Proctor, C., Gilmour, M., Pons-Branchu, E., Hamelin, B., 2001a. Dead carbon in stalagmites: carbonate bedrock paleodissolution vs ageing of soil organic matter. Implications for ¹³C variations in speleothems. *Geochimica et Cosmochimica Acta* 65, 3443–3457.
- Genty, D., Baker, A., Vokal, B., 2001b. Intra- and inter-annual growth rate of modern stalagmites. *Chemical Geology* 176(1–4), 191–212.
- Genty, D., Blamart, D., Ouahdi, R., Gilmour, M., 2003. Precise dating of Dansgaard-Oeschger climate oscillations in western Europe from stalagmite data. *Nature* 421, 833–837.
- Grant, K.M., Grimm, R., Mikolajewicz, U., Marino, G., Ziegler, M., Rohling, E.J., 2016. The timing of Mediterranean sapropel deposition relative to insolation, sea-level and African monsoon changes. *Quaternary Science Reviews* 140, 125e141.
- Grant, K.M., Rohling, E.J., Bar-Matthews, M., Ayalon, A., Medina-Elizalde, M., Bronk Ramsey, C., Satow, C., Roberts, A.P., 2012. Rapid coupling between ice volume and polar temperature over the past 150 ka. *Nature* 491, 744–747.
- Hajjar, L., Haïdar-Boustani, M., Khater, C., Cheddadi, R., 2010. Environmental changes in Lebanon during the Holocene: man vs. climate impacts. *Journal of Arid Environments* 74, 746–755.
- Hellstrom, J.C., McCulloch, M.T., 2000. Multi-proxy constraints on the climatic significance of trace element records from a New Zealand speleothem. *Earth and Planetary Science Letters* 179, 287–297.
- Huang, H.M., Fairchild, I.J., Borsato, A., Frisia, S., Cassidy, N.J., McDermott, F., Hawkesworth, C.J., 2001. Seasonal variations in Sr, Mg and P in modern speleothems (Grotta di Ernesto, Italy). *Chemical Geology* 175, 429–448.
- Jacobson, M.J., Flohr, P., Gascoigne, A., Leng, M.J., Sadekov, A., Cheng, H., Fleitmann, D., 2021. Heterogeneous late Holocene climate in the Eastern Mediterranean—the Kocain Cave record from SW Turkey. *Geophysical Research Letters* 48, e2021GL094733.
- Jaffey, A.H., Flynn, K.F., Glendenin, L.E., Bentley, W.T., Essling, A.M., 1971. Precision measurement of half-lives and specific activities of U 235 and U 238. *Physical Review C* 4(5), 1889.
- Jamieson, R.A., Baldini, J.U., Brett, M.J., Taylor, J., Ridley, H.E., Ottley, C.J., Pruffer, K.M., *et al.*, 2016. Intra- and inter-annual uranium concentration variability in a Belizean stalagmite controlled by prior aragonite precipitation: a new tool for reconstructing hydro-climate using aragonitic speleothems. *Geochimica et Cosmochimica Acta* 190, 332–346.
- Jochum, K.P., Pfänder, J., Woodhead, J.D., Willbold, M., Stoll, B., Herwig, K., Hofmann, A.W., 2005. MPI-DING glasses: new geological reference materials for in situ Pb isotope analysis. *Geochemistry, Geophysics, Geosystems* 6(10), 1–15.
- Jochum, K.P., Scholz, D., Stoll, B., Weis, U., Wilson, S.A., Yang, Q., Andrae, M.O., 2012. Accurate trace element analysis of speleothems and biogenic calcium carbonates by LA-ICP-MS. *Chemical Geology* 318, 31–44.
- Jones, M.D., Roberts, C.N., 2008. Interpreting lake isotope records of Holocene environmental change in the Eastern Mediterranean. *Quaternary International* 181, 32–38.
- Kallel, N., Duplessy, J.-C., Labeyrie, L., Fontugne, M., Paterne, M., Montacer, M., 2000. Mediterranean pluvial periods and sapropel formation during the last 200,000 years. *Palaeogeography, Palaeoclimatology, Palaeoecology* 157, 45–58.
- Keinan, J., Bar-Matthews, M., Ayalon, A., Zilberman, T., Agnon, A., Frumkin, A., 2019. Paleoclimatology of the Levant from Zalmon Cave speleothems, the northern Jordan Valley, Israel. *Quaternary Science Reviews* 220, 142–153.
- Kim, S.T., O’Neil, J.R., 1997. Equilibrium and nonequilibrium oxygen isotope effects in synthetic carbonates. *Geochimica et Cosmochimica Acta* 61, 3461–3475.
- Koeniger, P., Margane, A., Abi-Rizk, J., Himmelsbach, T., 2017. Stable isotope based mean catchment altitudes of springs in the Lebanon Mountains. *Hydrological Processes* 21, 3708–3718.
- Masson-Delmotte, V., Schulz, M., Abe-Ouchi, A., Beer, J., Ganopolski, A., Gonzalez Rouco, J.F., Jansen, E., *et al.*, 2013. Information from Paleoclimate Archives. In: *Climate Change 2013: The Physical Science Basis: Contribution of Working Group I to the Fifth Assessment Report of*

- the Intergovernmental Panel on Climate Change. Cambridge: Cambridge University Press, pp. 383–464.
- Matthews, A., Affek, H. P., Ayalon, A., Vonnhof, H. B., Bar-Matthews, M. 2021. Eastern Mediterranean climate change deduced from the Soreq Cave fluid inclusion stable isotopes and carbonate clumped isotopes record of the last 160 ka. *Quaternary Science Reviews* 272, 107223.
- McDermott, F., 2004. Palaeoclimate reconstruction from stable isotope variations in speleothems: a review. *Quaternary Science Reviews* 23, 901–918.
- Migowski, C., Stein, M., Prasad, S., Negendank, J.F.W., Agno, A., 2006. Holocene climate variability and cultural evolution in the Near East from the Dead Sea sedimentary record. *Quaternary Research* 66, 421–431.
- Mischel, S.A., Scholz, D., Spötl, C., Jochum, K.P., Schröder-Ritzrau, A., Fiedler, S., 2017. Holocene climate variability in Central Germany and a potential link to the polar North Atlantic: a replicated record from three coeval speleothems. *Holocene* 27, 509–525.
- Nader, F.H., Abdel-Rahman, A.F.M., Haidar, A.T., 2006. Petrographic and chemical traits of Cenomanian platform carbonates (central Lebanon): implications for depositional environments. *Cretaceous Research* 27, 689–706.
- Nehme, C., Kluge, T., Verheyden, S., Nader, F., Charalambidou, I., Weissbach, T., Gucel, S. et al. 2020. Speleothem record from Pentadactylos cave (Cyprus): new insights into climatic variations during MIS 6 and MIS 5 in the Eastern Mediterranean. *Quaternary Science Reviews*, 250, 106663.
- Nehme, C., Verheyden, S., Breitenbach, S.F., Gillikin, D.P., Verheyden, A., Cheng, H., Noble, S., et al., 2018. Climate dynamics during the penultimate glacial period recorded in a speleothem from Kanaan Cave, Lebanon (central Levant). *Quaternary Research* 90, 10–25.
- Nehme, C., Verheyden, S., Nader, F.H., Adjizian-Gerard, J., Genty, D., De Bont, K., Claves, P., 2019. Cave dripwater isotopic signals related to the altitudinal gradient of Mt. Lebanon: implication for speleothem studies. *International Journal of Speleology* 48, 1–8.
- Nehme, C., Verheyden, S., Noble, S.R., Farrant, A.R., Sahy, D., Hellstrom, J., Delannoy, J.J., Claves, P., 2015. Reconstruction of MIS 5 climate in the central Levant using a stalagmite from Kanaan Cave, Lebanon. *Climate of the Past* 11, 1785–1799.
- Orland, I.J., Burstyn, Y., Bar-Matthews, M., Kozdon, R., Ayalon, A., Matthews, A., Valley, J.W., 2014. Seasonal climate signals (1990–2008) in a modern Soreq Cave stalagmite as revealed by high-resolution geochemical analysis. *Chemical Geology* 363, 322–333.
- Regattieri, E., Zanchetta, G., Isola, I., Zanella, E., Drysdale, R.N., Hellstrom, J.C., Zerbini, A., et al. 2019. Holocene Critical Zone dynamics in an Alpine catchment inferred from a speleothem multiproxy record: disentangling climate and human influences. *Scientific Reports* 9, 17829.
- Roberts, M.S., Smart, P.L., Baker, A., 1998. Annual trace element variations in a Holocene speleothem. *Earth and Planetary Science Letters* 154, 237–246.
- Roberts, N., Eastwood, W.J., Kuzucuoğlu, C., Fiorentino, G., Caracuta, V., 2011. Climatic, vegetation and cultural change in the Eastern Mediterranean during the mid-Holocene environmental transition. *Holocene* 21, 147–162.
- Robinson, S.A., Black, S., Sellwood, B.W., Valdes, P.J., 2006. A review of palaeoclimates and palaeoenvironments in the Levant and eastern Mediterranean from 25 to 5 ka BP: setting the environmental background for the evolution of human civilisation. *Quaternary Science Reviews* 25, 1517–1541.
- Rohling, E.J., Cane, T.R., Cooke, S., Sprovieri, M., Bouloubassi, I., Emeis, K.C., Schiebel, R., et al., 2002. African monsoon variability during the previous interglacial maximum. *Earth and Planetary Science Letters* 202, 61–75.
- Rosignol-Strick, M., Paterne, M., 1999. A synthetic pollen record of the eastern Mediterranean sapropels of the last 1 Ma: implications for the time-scale and formation of sapropels. *Marine Geology* 153, 221–237.
- Rowe, P.J., Mason, J.E., Andrews, J.E., Marca, A.D., Thomas, L., van Calsteren, P., Jex, C.N., Vonnhof, H.B., Al-Omari, S., 2012. Speleothem isotopic evidence of winter rainfall variability in northeast Turkey between 77 and 6 ka. *Quaternary Science Reviews* 45, 60–72.
- Rozanski, K., Araguas, L., Gonfiantini, R., 1993. Isotopic patterns in modern global precipitation. In: Swart, P.K., Lohmann, K.C., McKenzie, J., Savin, S. (Eds.), *Climate Change in Continental Isotopic Records*. Geophysical Monograph Series 78. Washington, DC: American Geophysical Union, pp. 1–37.
- Saad, Z., Kazpard, V., El Samrani, A.G., Slim, K., 2005. Chemical and isotopic composition of rainwater in coastal and highland regions in Lebanon. *Journal of Environmental Hydrology* 13, 1–11.
- Scholz, D., Hoffmann, D.L., 2011. StalAge—an algorithm designed for construction of speleothem age models. *Quaternary Geochronology* 6, 369–382.
- Scrivner, A.E., Vance, D., Rohling, E.J., 2004. New neodymium isotope data quantify Nile involvement in Mediterranean anoxic episodes. *Geology* 32, 565–568.
- Şekeryapan, C., Streuman, H.J., van der Plicht, J., Woldring, H., van der Veen, Y., Boomer, I., 2020. Late Glacial to mid-Holocene lacustrine ostracods from S. Anatolia, Turkey: a palaeoenvironmental study with pollen & stable isotopes. *Catena* 188, 5–11.
- Shabaan, A., Houhou, R., 2015. Drought or humidity oscillations? The case of coastal zone of Lebanon. *Journal of Hydrology* 529, 1768–1775.
- Sinclair, D.J., Banner, J.L., Taylor, F.W., Partin, J., Jensen, J., Mylroie, J., Milkvič, B., 2012. Magnesium and strontium systematics in tropical speleothems from the Western Pacific. *Chemical Geology* 294, 1–17.
- Sinha, A., Kathayat, G., Weiss, H., Li, H., Cheng, H., Reuter, J., Edwards, R.L., 2019. Role of climate in the rise and fall of the Neo-Assyrian Empire. *Science Advances* 5, 11, 6656.
- Telesca, L., Shaban, A., Gascoïn, S., Darwich, T., Drapeau, L., El Hage, M., Faour, G., 2014. Characterization of the time dynamics of monthly satellite snow cover data on Mountain Chains in Lebanon. *Journal of Hydrology* 519, 3214–3222.
- Tooth, A.F., Fairchild, I.J., 2003. Soil and karst aquifer hydrological controls on the geochemical evolution of speleothem-forming drip waters, Crag Cave, southwest Ireland. *Journal of Hydrology* 273, 51–68.
- Torfstein, A., Goldstein, S.L., Kagan, E.J., Stein, M., 2013b. Integrated multi-site U–Th chronology of the last glacial Lake Lisan. *Geochimica et Cosmochimica Acta* 104, 210–231.
- Torfstein, A., Goldstein, S.L., Stein, M., Enzel, Y., 2013a. Impacts of abrupt climate changes in the Levant from Last Glacial Dead Sea levels. *Quaternary Science Reviews* 69, 1–7.
- Treble, P., Shelley, J.M.G., Chappell, J., 2003. Comparison of high resolution sub-annual records of trace elements in a modern (1911–1992) speleothem with instrumental climate data from SW Australia. *Earth and Planetary Science Letters* 216, 141–153.
- Tremaine, D.M., Froelich, P.N., Wang, Y., 2011. Speleothem calcite formed in situ: modern calibration of $\delta^{18}\text{O}$ & $\delta^{13}\text{C}$ paleoclimate proxies in a continuously monitored natural cave system. *Geochimica et Cosmochimica Acta* 75, 4929–4950.
- Ulbrich, U., Lionello, P., Belusic, D., Jacobeit, J., Knippertz, P., Kuglitsch, F.G., Leckebusch, G.C., et al., 2012. Climate of the Mediterranean: synoptic patterns, temperature, precipitation, winds, and their extremes. In: Lionello, P. (Ed.), *The Climate of the Mediterranean Region: From the Past to the Future*. Amsterdam: Elsevier, pp. 301–346.
- Ünal-İmer, E., Shulmeister, J., Zhao, J.X., Uysal, I.T., Feng, Y.X., Nguyen, A.D., Yüce, G., 2015. An 80 ka long continuous speleothem record from Dim Cave, SW Turkey with paleoclimatic implications for the Eastern Mediterranean. *Scientific Reports* 5, 13560.
- Van Zeist, W., Woldring, H., 1980. Holocene vegetation and climate of north-western Syria. *Palaeohistoria* 22, 111–125.
- Verheyden, S., Keppens, E., Fairchild, I.J., McDermott, F., Weis, D., 2000. Mg, Sr and Sr isotope geochemistry of a Belgian Holocene speleothem: implications for paleoclimate reconstructions. *Chemical Geology* 169, 131–144.
- Verheyden, S., Nader, F.H., Cheng, H.J., Edwards, L.R., Swennen, R., 2008. Paleoclimate reconstruction in the Levant region from the geochemistry of a Holocene stalagmite from the Jeita cave, Lebanon. *Quaternary Research* 70, 368–381.
- Weissbach, T., Kluge, T., Affolter, S., Leuenberger, M. C., Vonnhof, H., Riechelmann, D.F., Fohlmeister, J. 2023. Constraints for precise and accurate fluid inclusion stable isotope analysis using water-vapour saturated CRDS techniques. *Chemical Geology*, 617, 121268.
- Xoplaki, E., González-Rouco, J.F., Luterbacher, J., Wanner, H., 2004. Wet season Mediterranean precipitation variability: influence of large-scale dynamics and trends. *Climate Dynamics* 23, 63–78.
- Yasuda, Y., Kitagawa, H., Nakagawa, T., 2000. The earliest record of major anthropogenic deforestation in the Ghab Valley, northwest Syria: a palynological study. *Quaternary International* 73, 127–136.
- Ziv, B., Saaroni, H., Romem, M., Heifetz, E., Harnik, N., Baharad, A., 2010. Analysis of conveyor belts in winter Mediterranean cyclones. *Theoretical and Applied Climatology* 99, 441–455.